1.0

1.1

1.25   1.4   1.6

2.8   2.5

3.2   2.2

3.6

4.0   2.0

1.8

MICROCOPY RESOLUTION TEST CHART

NATIONAL BUREAU OF STANDARDS-1963

FG

AD A031124

SCHOOL OF MECHANICAL ENGINEERING
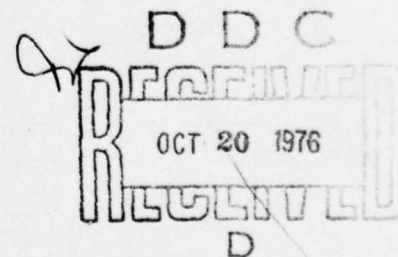
PURDUE UNIVERSITY

WEST LAFAYETTE, INDIANA 47907

(10)

SOLID MECHANICS AND MATERIALS
Laboratory

FATIGUE CRACK CLOSURE BEHAVIOR:
A COMPARATIVE STUDY

J. E. Rueping

B. M. Hillberry

D D C

OCT 20 1976

August 1976

Qualified requestors may obtain additional copies from the Defense
Documentation Center, all others should apply to the National Technical Information Service.

AIR FORCE OFFICE OF SCIENTIFIC RESEARCH (AFSC)
NOTICE OF TRANSMITTAL TO DDC
This technical report has been reviewed and is
approved for public release IAW AFR 190-12 (7b).
Distribution is unlimited.
A. D. BLOSE
Technical Information Officer

Conditions of Reproduction

Reproduction, translation, publication, use and disposal in whole or
in part by or for the United States Government is permitted.

SECURITY CLASSIFICATION OF THIS PAGE (When Data Entered)

REPORT DOCUMENTATION PAGE		READ INSTRUCTIONS BEFORE COMPLETING FORM
1. REPORT NUMBER AFOSR-TR-76-1090	2. GOVT ACCESSION NO.	3. RECIPIENT'S CATALOG NUMBER
4. TITLE (and Subtitle) FATIGUE CRACK CLOSURE BEHAVIOR: A COMPARATIVE STUDY		5. TYPE OF REPORT & PERIOD COVERED FINAL rept. 15 June 1975-14 August 1976
		6. PERFORMING ORG. REPORT NUMBER
7. AUTHOR(s) J. E. RUEPING B. M. HILLBERRY		8. CONTRACT OR GRANT NUMBER(s) AFOSR-75-2852 NEW
9. PERFORMING ORGANIZATION NAME AND ADDRESS PURDUE UNIVERSITY SCHOOL OF MECHANICAL ENGINEERING WEST LAFAYETTE, INDIANA 47907		10. PROGRAM ELEMENT, PROJECT, TASK AREA & WORK UNIT NUMBERS 681307 9782-05 61102F
11. CONTROLLING OFFICE NAME AND ADDRESS AIR FORCE OFFICE OF SCIENTIFIC RESEARCH/NA BLDG 410 BOLLING AIR FORCE BASE, D C 20332		12. REPORT DATE August 1976
		13. NUMBER OF PAGES 102
14. MONITORING AGENCY NAME & ADDRESS(if different from Controlling Office) AF-AFOSR-2852-75		15. SECURITY CLASS. (of this report) UNCLASSIFIED
		15a. DECLASSIFICATION/DOWNGRADING SCHEDULE

16. DISTRIBUTION STATEMENT (of this Report)
AF-9782 9782 05

Approved for public release; distribution unlimited.

17. DISTRIBUTION STATEMENT (of the abstract entered in Block 20, if different from Report)

18. SUPPLEMENTARY NOTES

19. KEY WORDS (Continue on reverse side if necessary and identify by block number)

FATIGUE   OVERLOAD
CRACK CLOSURE
LASER INTERFEROMETRY
ELBER GAGE
DELAY

20. ABSTRACT (Continue on reverse side if necessary and identify by block number)
Fatigue crack closure behavior in 2024-T3 aluminum alloy was investigated using a laser interferometry method developed in this investigation and an "Elber" type displacement gage. The crack closure results using the two measurement methods are compared for constant amplitude loading. The displacement gage was also used to measure the crack closure behavior following selected overload/underload sequences. These results are compared with an "inverse" technique. The measurement methods and equipment are described and the crack closure results are presented.

DD FORM 1473 1 JAN 73   EDITION OF 1 NOV 65 IS OBSOLETE

292070   SECURITY CLASSIFICATION OF THIS PAGE (When Data Entered)

ACKNOWLEDGMENTS

TABLE OF CONTENTS

Page

LIST OF TABLES

LIST OF FIGURES

LIST OF SYMBOLS

A	cross-sectional area of specimen
a	crack length
a_{OL}	crack length at which overload/underload was applied
b	constant
C	constant
d	slit or indentation separation
$\dfrac{da}{dN}$	crack growth rate
$\dfrac{d^2S}{d\delta^2}$	curvature in stress versus displacement relation
E	Young's modulus
K_{MAX}	maximum cyclic stress intensity
K_{MIN}	minimum cyclic stress intensity
K_{OL}	overload stress intensity
K_{OP}	opening stress intensity
K_{UL}	underload stress intensity
L	light source
m	fringe order
N	number of cycles
n	constant
P	fixed observation point

P_{MAX} maximum cyclic load

P_{OP} crack opening load

Q_{OL} ratio of K_{OL}/K_{MAX}

R optical path length from a point midway between the indentations to the fixed observation point, P.

R_{CAL} value of calibration resistance

R_{COMP} resistance in compensating arm of bridge network

R_F stress intensity ratio, K_{MIN}/K_{MAX}

R_M ratio of K_{MIN}/K_{OL}

R_{UO} ratio of K_{UL}/K_{OL}

r_y calculated plastic zone radius

S stress

S_{MAX} maximum cyclic stress

S_{MIN} *minimum cyclic stress*

S_{OP} crack opening stress

U $\dfrac{K_{MAX}-K_{OP}}{K_{MAX}-K_{MIN}}$

U_{OL} $\dfrac{K_{OL}-K_{OP}}{K_{OL}-K_{UL}}$

X horizontal component of R

Y vertical component of R

α constant

γ angle

ΔL phase shift due to rigid body motion

ΔK $K_{MAX}-K_{MIN}$

ΔK_{EFF} effective stress intensity range, $K_{MAX}-K_{OP}$

ΔR phase shift due to slit or indentation separation

ΔS	$S_{MAX} - S_{MIN}$
δ	displacement
δd	change in displacement between the indentations
δm	number of fringes or fractions thereof passing the point of observation
$\delta\theta$	fringe spacing
ε	strain
ε_{CAL}	strain simulated during shunt calibration
$\varepsilon_{Elastic}$	maximum strain elastic
θ	angle measured from the normal to the plane containing the slits (indentations) to a line from the point midway between the slits (indentations) to the observation point, P.
θ_o	fixed observation angle
λ	wavelength of light
σ_{ys}	yield strength of material
ϕ	angle

INTRODUCTION

In recent years considerable effort has been devoted to gaining an understanding of fatigue crack propagation. The introduction of fracture mechanics into the fatigue design process has provided the impetus for understanding fatigue crack propagation and for the development of adequate crack propagation prediction techniques. It is not uncommon for nearly all of the life of a part to be taken up by the crack propagation phase of the fatigue process. The load interaction effects complicate prediction of the crack growth behavior. Although several models have been proposed to account for interaction effects [1,2][1] this is still of primary concern in assessing the life of a structure. The crack closure model [3,4] has been used to qualitatively describe load interaction effects, however it is difficult to measure crack opening loads.

In this investigation a laser interferometric technique was developed to measure the crack edge displacements from which crack closure is determined. This technique, capable of giving continuous measurements, was used to measure the crack closure behavior in 2024-T3 aluminum alloy for constant amplitude loading. These results are compared with crack closure measurements using an "Elber" type displacement gage. In addition, the "Elber" gage was used to investigate crack closure behavior following selected overload/underload sequences. These results are compared directly with an "inverse" technique for determining crack closure.

---

[1]Numbers in brackets refer to references listed in the Bibliography.

REVIEW OF LITERATURE

Elber [3,4] observed that fatigue cracks in aluminum alloy close while still subjected to a tensile load. He also further observed that significant compressive stresses are transmitted across the crack at zero load. Fatigue crack opening behavior is often explained by analogy to a zero width saw-cut. An important difference is that a zone of residual tensile deformation is left in the wake of the advancing crack tip. These deformations actually decrease the amount of crack opening displacement from that of a saw-cut crack. Upon unloading, this can result in crack closure above zero load. This closure stress at zero load level must be overcome before the crack surfaces can physically separate allowing propagation. Thus, the effective range of cyclic loading is reduced. Peak overloads cause the local plastic zone of deformation to change size which in turn alters the closure stresses and thus perturbs subsequent crack growth.

Since the Elber closure model offers the potential for explaining many of the load interaction effects observed in fatigue crack propagation, considerable research effort has recently been directed toward applying a closure based model to fatigue crack propagation behavior following overloads [5,6,7].

Fatigue crack propagation behavior for constant amplitude loading has been characterized reasonably well in terms of the stress intensity

range, ΔK, as [8]

$$\frac{da}{dN} = C\ (\Delta K)^n \tag{1}$$

where

  a = crack length

  N = number of cycles

  ΔK = stress intensity range, $K_{MAX} - K_{MIN}$

  C = constant

  n = constant

This expression has been modified to account for the increased growth rate which accompanies higher values of the mean stress intensity level. In terms of the stress ratio effect, characterized by the ratio of the minimum stress intensity to the maximum stress intensity during the cycle, $R_F = K_{MIN}/K_{MAX}$, Equation 1 can now be written as

$$\frac{da}{dN} = C\ (\Delta K_{EFF})^n \tag{2}$$

where

  ΔK_{EFF} = effective stress intensity range producing crack growth. This is generally a function of at least ΔK and R_F. The exact form which ΔK_{EFF} should take to best account for the observed phenomena is subject to some debate. In each case, however, it is significant that the applied stress intensity range, ΔK, which is the difference between the maximum applied cyclic stress intensity and the minimum applied cyclic stress intensity, is greater than the range which effectively propagates the crack, ΔK_{EFF}. This implies that only a portion of the available energy is being used for fatigue crack propagation.

CRACK CLOSURE

Elber [3,4] first proposed the mechanism of crack closure as a possible explanation of fatigue crack propagation under constant amplitude loading. Permanent tensile deformation causing incompatibility of the fracture surfaces and residual compressive stresses are believed to be responsible for fixing the level of opening well above the zero level for tension-tension loading. Elber observed that the crack surfaces were closed over a significant portion of the tensile loading cycle and suggested that crack extension was not possible which the crack was closed. This lead Elber to defining the effective level of stress propagating a fatigue crack as $S_{MAX} - S_{OP}$, where S_{OP} is the applied stress level at which the crack opens. Thus in terms of stress intensities, K,

$$\Delta K_{EFF} = K_{MAX} - K_{OP} \tag{3}$$

where

K_{OP} = the opening stress intensity

Substituting into Equation 2,

$$\frac{da}{dN} = C \left(K_{MAX} - K_{OP} \right)^n \tag{4}$$

Elber defined a quantity U as,

$$U = \frac{S_{MAX} - S_{OP}}{\Delta S} \tag{5}$$

or

$$U = \frac{K_{MAX} - K_{OP}}{\Delta K} \tag{6}$$

Then Equation 4 becomes

$$\frac{da}{dN} = C \ (U \ \Delta K)^n \tag{7}$$

Elber measured crack opening in a series of constant amplitude loading tests to determine the functional form of U. Assuming possible correlation with R_F, ΔK, and a, he found only R_F was significant. From experimental results for 2024-T3 aluminum alloy Elber found $U = 0.5 + 0.4 \ R_F$ [4]. More recent work by Shih and Wei [9,10] with titanium Ti 6 AL-4V alloy suggests that U is also dependent on K_{MAX}.

Load interactions can be treated with this theory by considering K_{OP} in Equation 4 as the parameter which varies with crack growth rate. For a single overload cycle, the overload reduces the growth rate, $\frac{da}{dN}$, which implies a reduction in the effective stress intensity level ΔK_{EFF}, or an increase in the opening stress intensity level K_{OP}. The variation of K_{OP} through the overload affected zone is shown qualitatively in Figure 1. According to the crack closure theory the plastic zone created by an overload will result in residual stresses in the material which tend to hold the crack closed. This closure action is reflected by higher values of the opening stress intensity K_{OP}.

A propagating crack has a region of plastic deformation at the crack tip which is known as the plastic zone, the size of which is determined by the magnitude of the loading. For a small load, the material deforms plastically but only in the plane of the specimen.
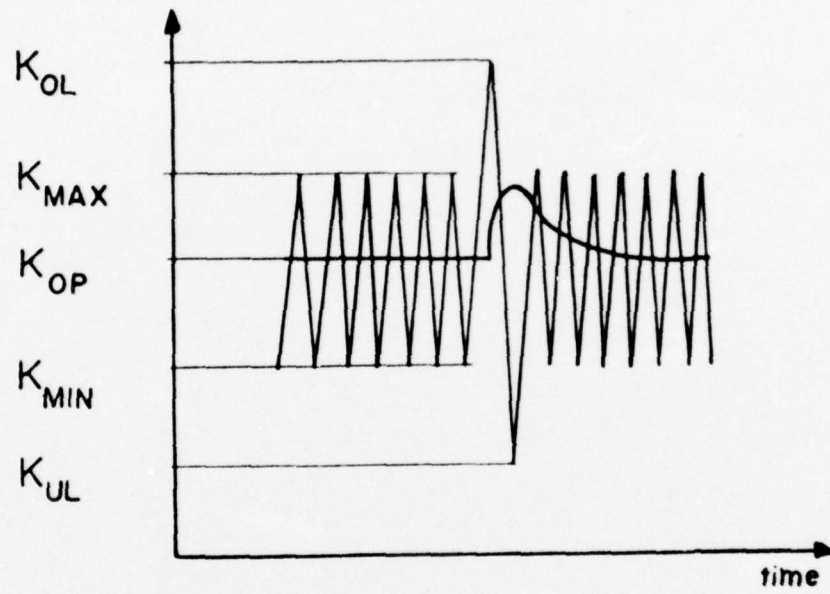
Figure 1   Qualitative Variation of Opening Stress Intensity Level
Due to an Overload/Underload Sequence [5]

This loading condition is referred to as plane strain. Application of higher loads results in three-dimensional deformation, and if the diameter of the plastic zone is greater than or equal to the specimen thickness, a state of plane stress exists. The diameter of the plastic zone is normally approximated by the following expression:

$$2r_y = \frac{1}{\alpha\pi} \left(\frac{K}{\sigma_{ys}}\right)^2 \tag{8}$$

where

r_y = radius of the plastic zone

K = maximum stress intensity

σ_{ys} = yield strength of the material

α = 1 for plane stress

α = 3 for plane strain

$1<\alpha<3$ for mixed mode

In the case of overloads and/or underloads applied to steady state fatigue cycling, the plastic zone diameter as calculated above has been shown to correlate with the observed load interaction zone [5,6,7,11]. Upon loading the stress at the crack tip can be reduced by no more than twice the yield stress of the material. Superposition of these effects results in a residual stress distribution which contributes to the crack closure behavior.

Significance of Stress vs. Displacement Relation

Elber [3,4] determined the crack opening stress by analyzing the nonlinearities in the relation between applied stress and crack edge displacements. This relationship was found experimentally using a gage, similar to the one used in this investigation, positioned on the surface of the specimen slightly behind the crack tip. See Figure 2. This nonlinear behavior can be the result of plastic deformation of the material or a change in configuration of the specimen. Elber identified the cause of the nonlinearity by analyzing the curvature of the stress displacement curve shown in Figure 2B. The relation is linear between points A and B and the measured stiffness is equal to the stiffness of the uncracked specimen. The stress displacement relation for the specimen without a crack is shown for comparison. The curve is also linear between points C and D with the measured stiffness equal to the measured stiffness of an identical sheet containing a saw-cut of the same length as the fatigue crack. The curvature, $\frac{d^2 S}{d\delta^2}$, between points B and C is negative. However, as plastic behavior of the material would produce a positive curvature on unloading, the only possible cause for a negative curvature is a change in configuration which increases the stiffness for decreasing loads. Elber explained this change in configuration as crack closure. Thus the crack is fully open between points D and C during unloading. The crack gradually closes between points C and B, and is closed between points B and A.

9
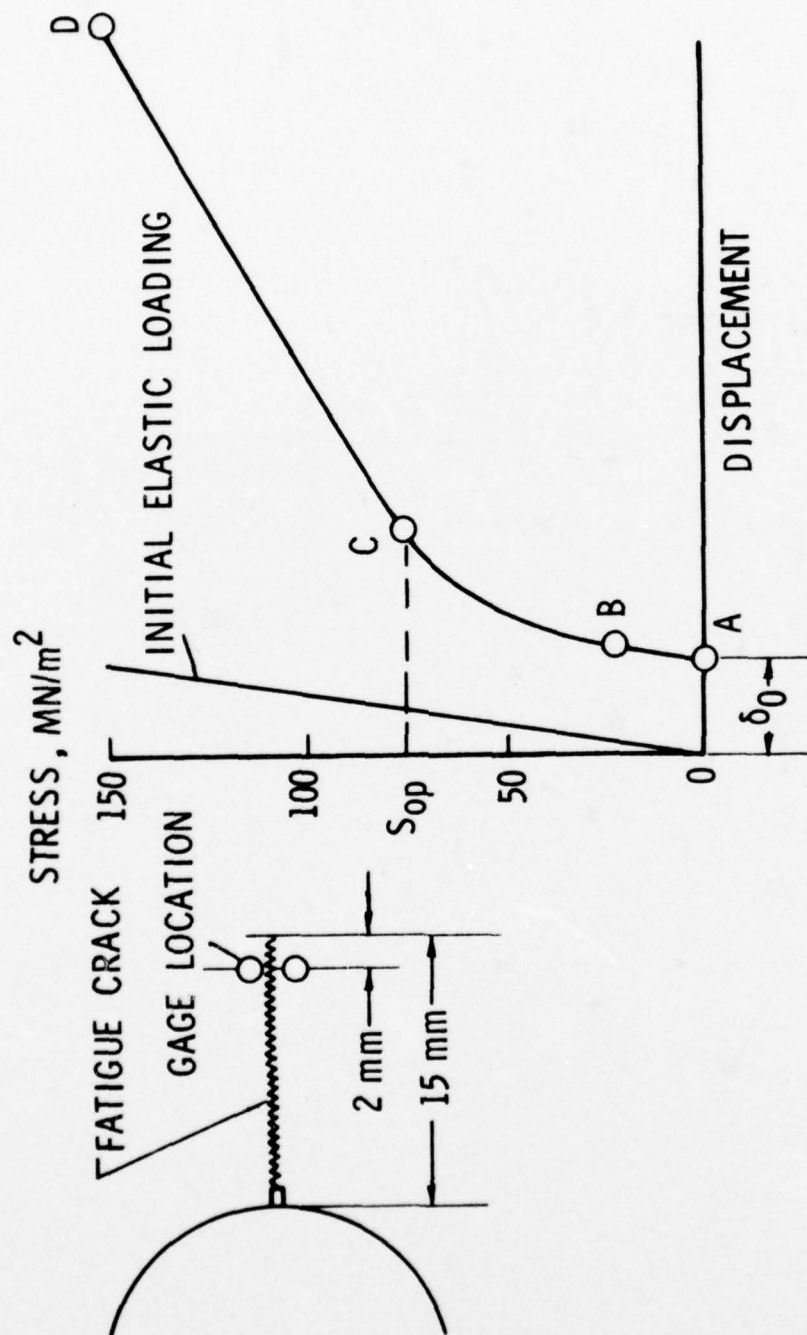
(a) CRACK CONFIGURATION   (b) APPLIED STRESS - DISPLACEMENT RELATION
AND GAGE LOCATION

Figure 2. Crack configuration and applied stress-displacement relationship[4]

Figure 3 shows that as the gage location approaches the crack tip the behavior measured is no longer fully elastic but has similarities with the behavior shown in Figure 2B. In Figure 3 a plastic deformation effect is superimposed on the configuration change effect. Between points A and B the curve is linear showing that the crack is closed. Between points B and C the negative curvature indicates that the crack is opening. Between points C and D the curve is linear, and between points D and E the curve again exhibits a negative curvature. The curvature between B and C is due entirely to crack opening, because plastic tensile deformations can only occur after the crack is fully open. The curvature between D and E is a result of plastic deformations in the plastic zone. Experimentally obtained curves are not always this well defined and the region from C to D may be relatively short compared to the total length of the curve, and a straight line portion cannot be identified. However, there must be a stress level at which the crack is fully open and at which the stiffness corresponds to the elastic stiffness of the fully open crack. This stiffness is obtained as the slope of the unloading branch at the maximum load of the previous cycle, where the crack is fully open and the material behaves elastically. A line with this slope can be used as a tangent to the loading branch to determine the crack opening load. When the tangency condition exists for some length of curve, the crack opening load is given by the lowest stress level satisfying the tangency condition. This is shown in Figure 3 where C represents the lowest tangency point. Figure 4 shows Elber's interpretations of curvatures for loading and unloading conditions [4].
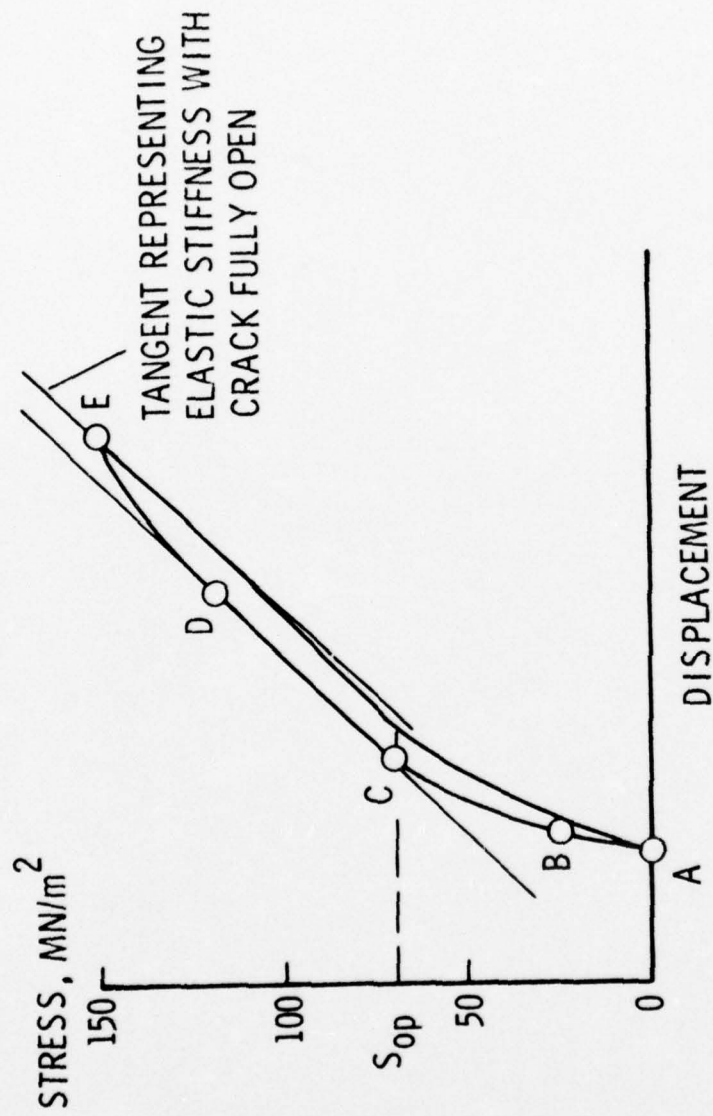
Figure 3. Relation between applied stress and gage displacement at the crack tip[4]

$\dfrac{d^2P}{d\delta^2}$	Shape	Loading	Unloading
I >0		Generally impossible for metals	1) Plastic behavior 2) Plastic behavior $>$ configuration change
II <0		1) Configuration change 2) Plastic behavior	1) Configuration change 2) Configuration change $>$ plastic behavior
III $=0$		Elastic behavior at constant configuration	1) Elastic behavior at constant configuration 2) Plastic behavior $=$ configuration change
IV $\to 0$		Transition from changing configuration to constant configuration	Transition to configuration change $>$ plastic behavior

Figure 4. Curvature effects in the load-displacement relation[4]

THE INVERSE METHOD

The inverse technique has been used to determine an effective K_{OP} following an overload/underload sequence. This requires the measurement of crack length, a, and the corresponding number of cycles, N, determining the growth rate and relating this to the constant amplitude growth rate. Alzos investigated the effects of single overload/ underload cycles on otherwise constant amplitude loading in terms of the following non dimensional parameters [5].

$$R_{UO} = \frac{K_{UL}}{K_{OL}}$$

$$R_M = \frac{K_{MIN}}{K_{OL}}$$

$$Q_{OL} = \frac{K_{OL}}{K_{MAX}}$$

where K_{OL} = overload stress intensity

K_{UL} = underload stress intensity

K_{MAX} = maximum cyclic stress intensity

K_{MIN} = minimum cyclic stress intensity

The overload/underload load cycling is illustrated in Figure 5. Selecting the value of each of these ratios and one stress intensity level (in this investigation K_{OL} = 33.33 Ksi $\sqrt{in}$) all other loading parameters (K_{MAX}, K_{MIN}, K_{UL}) are established. One goal of this
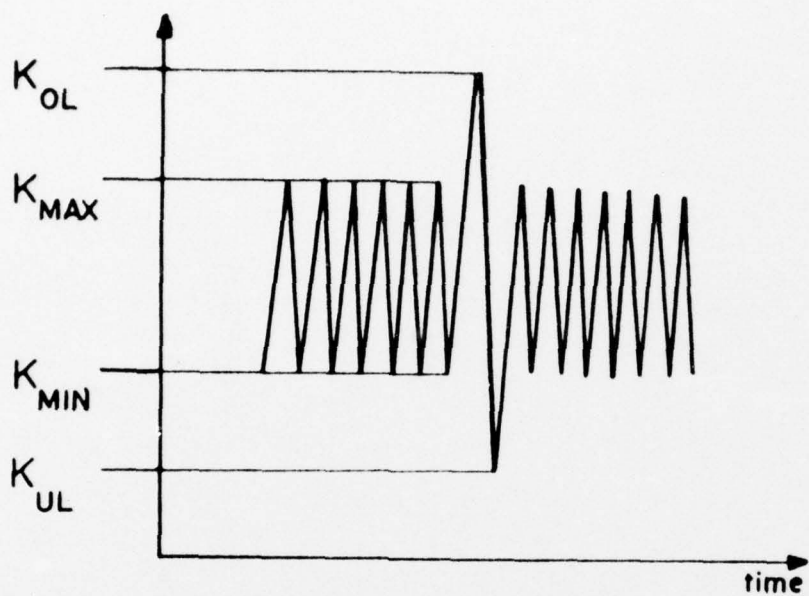
$$R_{UO} = \frac{K_{UL}}{K_{OL}} \qquad R_M = \frac{K_{MIN}}{K_{OL}}$$

$$R_F = \frac{K_{MIN}}{K_{MAX}} \qquad Q_{OL} = \frac{K_{OL}}{K_{MAX}}$$

Figure 5   Definition of variables [5]

investigation is to compare experimentally obtained values of K_{OP} obtained at discrete points throughout the overload affected zone with the value of K_{OP} predicted by the inverse technique.

In the inverse method a vs. N data is numerically differentiated by fitting a curve to the data which allows evaluation of the derivative at specific points. Recalling Equations 6 and 7

$$U = \frac{K_{MAX} - K_{OP}}{\Delta K} \tag{6}$$

and

$$\frac{da}{dN} = C \ (U \ \Delta K)^n \tag{7}$$

the constants C and n were then determined from a regression analysis.

Alzos originally compared the crack closure model with his results assuming that the overload cycles established the residual stress field in the vicinity of the crack tip and that it is not affected by subsequent cycling. This establishes the crack opening stress intensity level throughout the overload affected region. The functional form of U based on the definition of overload/underload parameters is:

$$U_{OL} = \frac{K_{OL} - K_{OP}^{MAX}}{K_{OL} - K_{UL}} \tag{9}$$

The functional form of U_{OL} in terms of the dimensionless ratios defining the overload/underload sequence was determined from the data by plotting: 1) U_{OL} VS. Q_{OL} for R_{UO} constant which predicted a linear Q_{OL} term, 2) U_{OL} VS. R_{UO} for Q_{OL} constant which showed that U_{OL} was second order in R_{UO}. The data were then correlated using a regression analysis to determine the constants for the following equation:

$$U_{OL} = C_1 + C_2 R_{UO} + C_3 R_{UO}^2 + C_4 Q_{OL} \tag{10}$$

Comparing this with the experimental data indicated that crack closure did in fact describe the observed behavior. Knowing U_{OL}, K_{OP}^{MAX} could be found by employing the following relationship

$$K_{OP}^{MAX} = K_{OL} [1 - (1 - R_{UO}) U_{OL}] \tag{11}$$

This permitted the minimum growth rate following an overload to be calculated:

$$\left. \frac{da}{dN} \right|_{MIN} = C (K_{MAX} - K_{OP}^{MAX})^n \tag{12}$$

Alzos [5] also developed an equation for predicting the number of delay cycles after a single overload/underload sequence.

The experimental $\left. \frac{da}{dN} \right|_{MIN}$, which can most easily be determined graphically, can be compared with the calculated values or can be used to predict K_{OP}^{MAX}. Having the minimum growth rate, Equation 12 can be solved for K_{OP}^{MAX}, which represents the maximum opening stress intensity. The inverse technique is shown schematically in Figure 6.

METHODS OF EXPERIMENTALLY MEASURING CRACK OPENING

The major problem encountered in measuring crack closure behavior is to experimentally determine when the crack surfaces physically separate under external load. The problem is difficult because of tunneling effects which cloud the precise definition of the crack front based on the visible edge. Secondly crack opening displacements in the vicinity of the crack tip are extremely small. Since this thesis presents a method permitting dynamic measurements of crack surface displacements, which are then used to determine K_{OP}, a brief review of alternate measurement techniques are presented.

$$K_{OP} = K_{MAX} - \Delta K_{EFF}$$
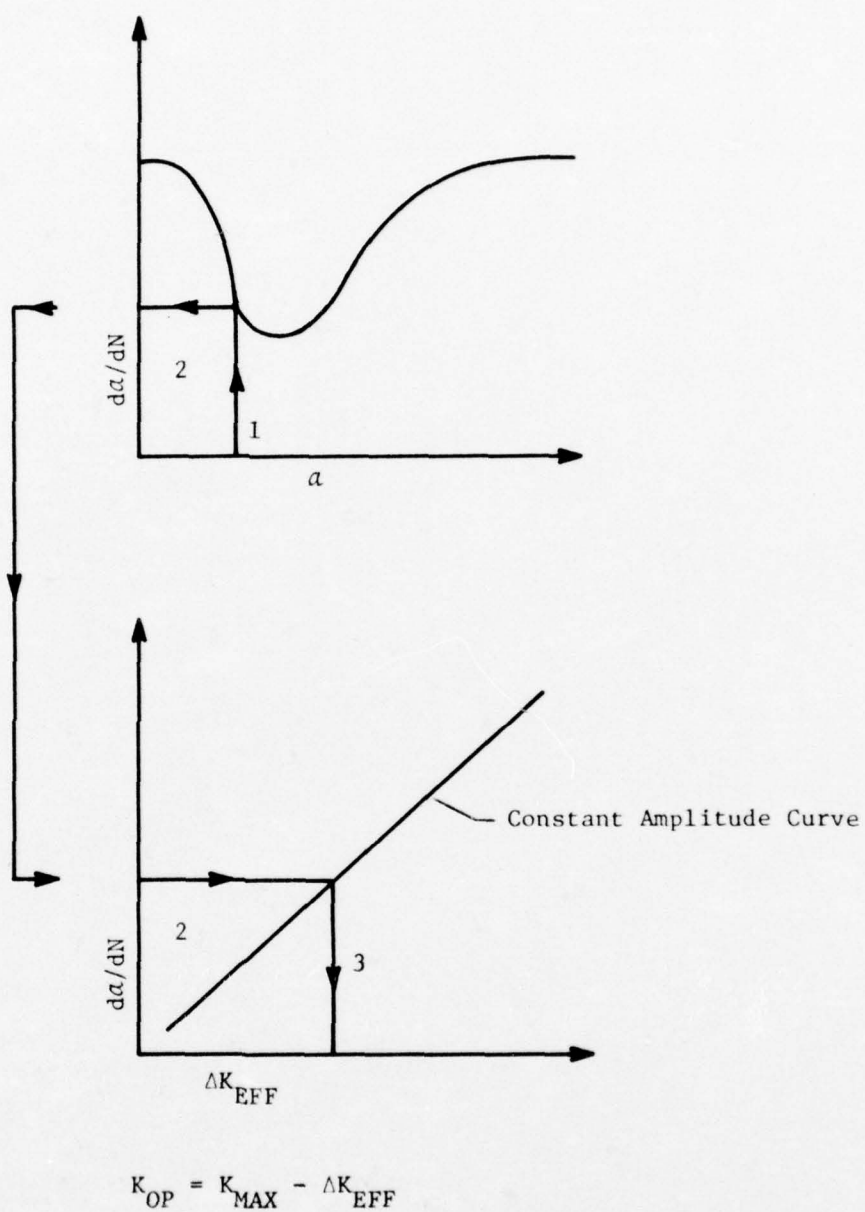
Figure 6   Schematic of Inverse Method for Determining K_{OP}.

Potential Drop

In this technique a constant current is fed through the specimen producing a potential drop between probe wires attached to the specimen surface on either side of the crack. Most of the D.C. component is "backed off" with a precision voltage source, while the remaining A.C. and D.C. components undergo some sort of amplification prior to recording. The change in potential can be related to changes in the projected surface area of the fatigue crack. In specimens of uniform thickness with no closure, the measured area is equivalent to crack length.

This technique has been used by Shih and Wei [9,10] and Irving et al., [12] to infer crack closure behavior from variations in crack area during the load cycle. The opening loads obtained by from this technique are consistently higher than those indicated by a strain gage extensiometer.

Ultrasonics

Buck, et al. [13] conducted retardation/closure studies in surface flawed aluminum specimens. Quasi-Raleigh surface waves were introduced ultrasonically to measure the size of the surface flaw. Upon loading, the apparent crack length increased to a threshold level, at which the flaw depth remained constant under further load. It was concluded from these measurements that the change in apparent crack length was due to separation of the initially compressed crack forces as suggested by Elber. While this ultrasonic technique is useful for specimens with part through cracks, the closure load is

inferred from a change in the average crack length, and not by a direct measurement of the crack edge profile.

Strain and Displacement Gages

A foil type strain gage applied to the specimen such that is straddles the crack edge profile can be used to monitor displacement as the crack propagates through the region of interest. In actuality one obtains the average crack edge displacement over the area covered by the gage [14].

Others have improved on the direct application of strain gages by using extensiometers which acting through knife edge or pin type mounts take advantage of multiple strain gages, temperature compensation, and high strain gage body geometries, which significantly improve the sensitivity and the accuracy [4,15,16].

Katcher and Kaplan [16] used two types of crack tip strain gages which attached to the specimen via hardened steel pins, the gages were held in position by spring tension. Closure loads were investigated in aluminum and titanium alloys from a series of load displacement records. Closure loads were obtained from load displacement curves as originally suggested by Elber.

Evidence for crack closure was obtained in Elbers original experiments [3,4] by a displacement transducer with gage length of 1.5 mm placed on the side of the specimen, straddling the crack. From changes in linearity in the output of load versus displacement records, Elber concluded that a significant portion of the loading cycle was required to overcome residual compressive stresses acting to prevent separation

of the crack faces. Since measurements were restricted to the displacement between fixed points, it was not possible to map the behavior along the entire crack profile.

Optical Measurement Techniques

Crack displacements were measured optically by Adams [17] in an investigation of through cracked aluminum sheets. Photomicrographs taken along a datum line ahead of the crack tip were magnified 4000x and used to define two distinctive surface marking approximately 0.076 mm apart. Once the fatigue crack had propagated between those reference marks, photographs were taken during the application of external loading. The load displacement record inferred from these photographs suggested that the crack was at least partially closed during a large portion of the tensile load cycle. The one short coming of this technique is that, measurements are restricted to the displacement of two fixed points.

Interferometry

Interferometry methods have been employed by several investigators to obtain the complete three-dimensional crack surface displacement field in transparent specimens. In particular Pitoniak et al. [18] used interferometry techniques to study crack closure in polymethyl-methacrylate specimens. Examination of the interference fringe patterns obtained for various loadings revealed that the crack perimeter was closed at zero load, but was displaced in the specimen interior. Although the fringe patterns provided a quantitative mapping of the entire crack surface profile, measurements by this method are restricted to transparent materials.

Sharpe [19] initiated the development of a laser interferometry technique which has the capability of measuring crack edge displacements continuously with a high degree of sensitivity (0.1 micron). Two parallel and uniform V-shaped grooves are made in the prepared specimen on either side of the initiated crack. These grooves cause light rays emanating from a laser source to be reflected (diffracted) at angles determined by groove geometry. Since laser radiation is monochromatic and coherent, optical interference patterns are formed in space. Sharpe fixes the observation angle and compares fringe shifts from fringe pattern photographs before and after the crack has opened or partially opened. The distance on the film that a fringe has moved is converted to a fringe shift value by dividing it by the original fringe spacing. Fringe motion gives a magnified picture of crack displacement. The standard of comparison is the fringe pattern emanating from the undeformed region in front of the crack tip.

This technique requires a fairly smooth flat surface. Grooves are made with a wedge shaped diamond adapted to a tool makers microscope.

This technique has been used successfully in studies of retardation [20], experimental stress intensity factor calibration [21], and the effects of rest time on retardation and observations of crack closure [22].

It is the intent of this work to verify the crack closure model by comparing calculated values of K_{OP} with direct measurements of K_{OP} by Elber gage and an interferometry based technique.

THE TEST PROGRAM

Constant Stress Amplitude Tests

The values of K_{OP} obtained from the Elber gage and the laser in-
terferometry method were compared for a series of constant stress
amplitude tests.

For these tests the maximum and maximum growth rates were se-
lected from Alzos' constant stress data as 5.0×10^{-7} in/cycle and
5.0×10^{-6} in/cycle. The da/dN vs. ΔK_{EFF} data bracketed by these
growth rates is very well defined. These growth rates gave approx-
imate upper and lower bounds for ΔK_{EFF}. Then choosing values of R_F,
based on the overload/underload test matrix used by Alzos, the range
of ΔK for each R_F was calculated. In this range four equally spaced
ΔK values were chosen as starting points. Thus a total of sixteen
constant amplitude tests were run over a Δa of approximately .500 mm,
with a vs. N data being taken to insure steady state conditions prior
to measuring the crack opening behavior. This test program is
shown in Table A-1 of Appendix A.

At slow growth rates $da/dN \approxeq 5 \times 10^{-7}$ the crack length was re-
corded at intervals of approximately 0.01 mm. Increments less than
0.01 mm would tend to introduce artificial scatter in the da/dN vs.
ΔK_{EFF} curve. At growth rates approaching approximately 5×10^{-6} in-
crements of 0.05 mm were used. The density at which the a vs. N data

could be acquired was limited by the rate at which the microscope traverse could be moved and the printer operated. Over the range of growth rates of interest it is estimated that the crack tip was located accurately within $\pm$ 0.005 mm.

The growth rate, da/dN, was determined from the raw a vs. N data using a seven point moveable strip technique. This method involves fitting a second order polynomial to seven consecutive data points using a least squares approach. This fitted function is differentiated and evaluated at the center of the interval. The strip is then advanced one point and the evaluation repeated. This process continues until the entire curve has been evaluated.

Overload/Underload Tests

One goal of this investigation was to measure K_{OP} at discrete points throughout the overload affected zone for a number of tests which gave good results using the inverse technique. Alzos' tests are shown in Table B-1 of Appendix B. From his original results, shown in Figures B-1, B-2, and B-3 also in Appendix B, tests 8, 11, 12, 13, 14, 15 and 18 were selected as being representative of expected K_{OP} values and therefore to measure K_{OP} experimentally.

All tests were performed with K_{OL} constant, consequently the effect of the overload level was not investigated. The overload level was chosen to insure a plane stress condition which requires that the plastic zone diameter, $2r_y$ be greater than the specimen thickness, thus:

$$2r_y = \frac{1}{\pi} \left(\frac{K_{OL}}{\sigma_{ys}}\right)^2 > 0.100 \text{ in} \tag{13}$$

where

> r_y = calculated plastic zone radius
>
> K_{OL} = overload stress intensity
>
> σ_{ys} = yield strength of material

These tests are numbered and shown in Figure 7.

For each test the specimen was cycled to establish steady state growth behavior, then the overload/underload sequence applied, and then cycling resumed at the pre-overload level. The steady state condition was achieved by propagating the fatigue crack at quasi-constant stress intensity, K, for a distance of at least 6 mm (over twice the diameter of the theoretical plastic zone of each test). The overload was then applied when the crack had propagated 5 percent past the point of the previous load shed. a vs. N data was taken as described previously.

One of the objectives of this study was to characterize growth rate behavior as well as K_{OP} through the overload affected zone, following the overload sequence. In order to obtain the growth rate, da/dN, throughout this overload zone it was necessary to record a vs. N with sufficient density and then differentiate these data.

Strip chart recordings of the Elber gage output and the load signal were taken at nonuniform intervals based on incremented changes in crack length after the overload. Insight into interval spacing was gained by plotting da/dN versus both a and N from Alzos' tests. These intervals were chosen such that K_{OP} data would be most dense in the immediate post overload portion of each test where da/dN changes most rapidly.
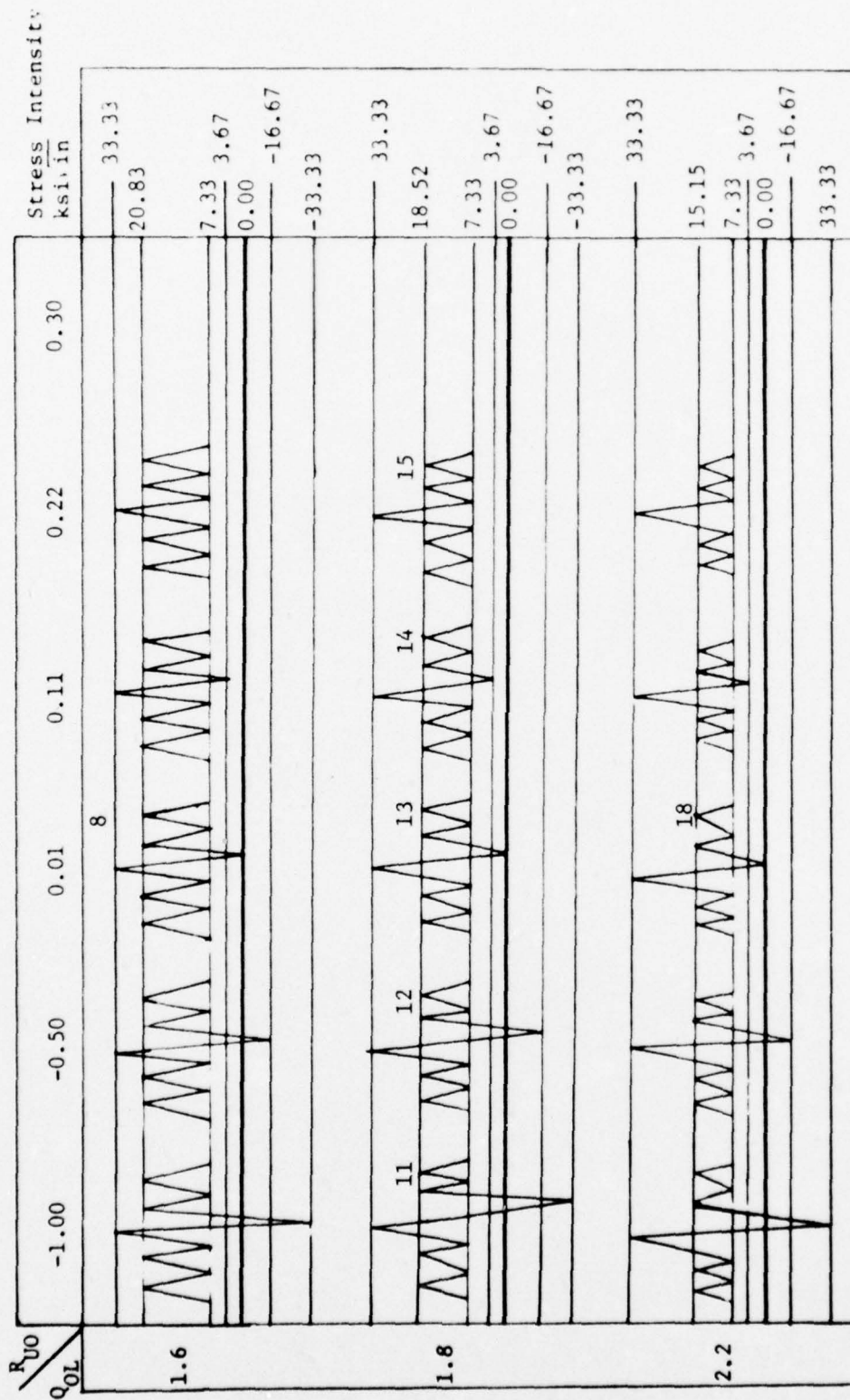
$R_M = 0.22$, K_{MIN} constant

Figure 7 Q_{OL} vs. R_{UO} test matrix [5]

EXPERIMENTAL INVESTIGATION

Test Specimen

The test specimens used in this investigation were 0.100 inch thick center crack panels of 2024-T3 aluminum alloy, identical to those used by Probst [23], Himmelein [24], Alzos [5], Skat [6], and Crandall [11]. The specimen geometry is shown in Figure 8. The material was from a new heat and the tensile properties were determined by testing three ASTM standard specimens. Average values appear in Table 1.

Test specimens were obtained with a mill finish and polished to a mirror finish in the vicinity of the crack path. This is an aid to optical observation of the crack tip and improves the quality and consistency of the diamond marks. The stress raiser was electrodischarge machined. Loading was applied parallel to the direction of rolling of the material. All tests were performed at room temperature and in laboratory air. Because of the necessity of repeated installation of the Elber gage it was not possible to enclose the sample with a dessicant in the vicinity of the crack as had been done by Alzos [5].

Test Equipment

The test machine was a 20 Kip electro-hydraulic, closed-loop system operated in load control. Load levels were accurately set using a digital voltmeter. Overloads and all data cycles were recorded
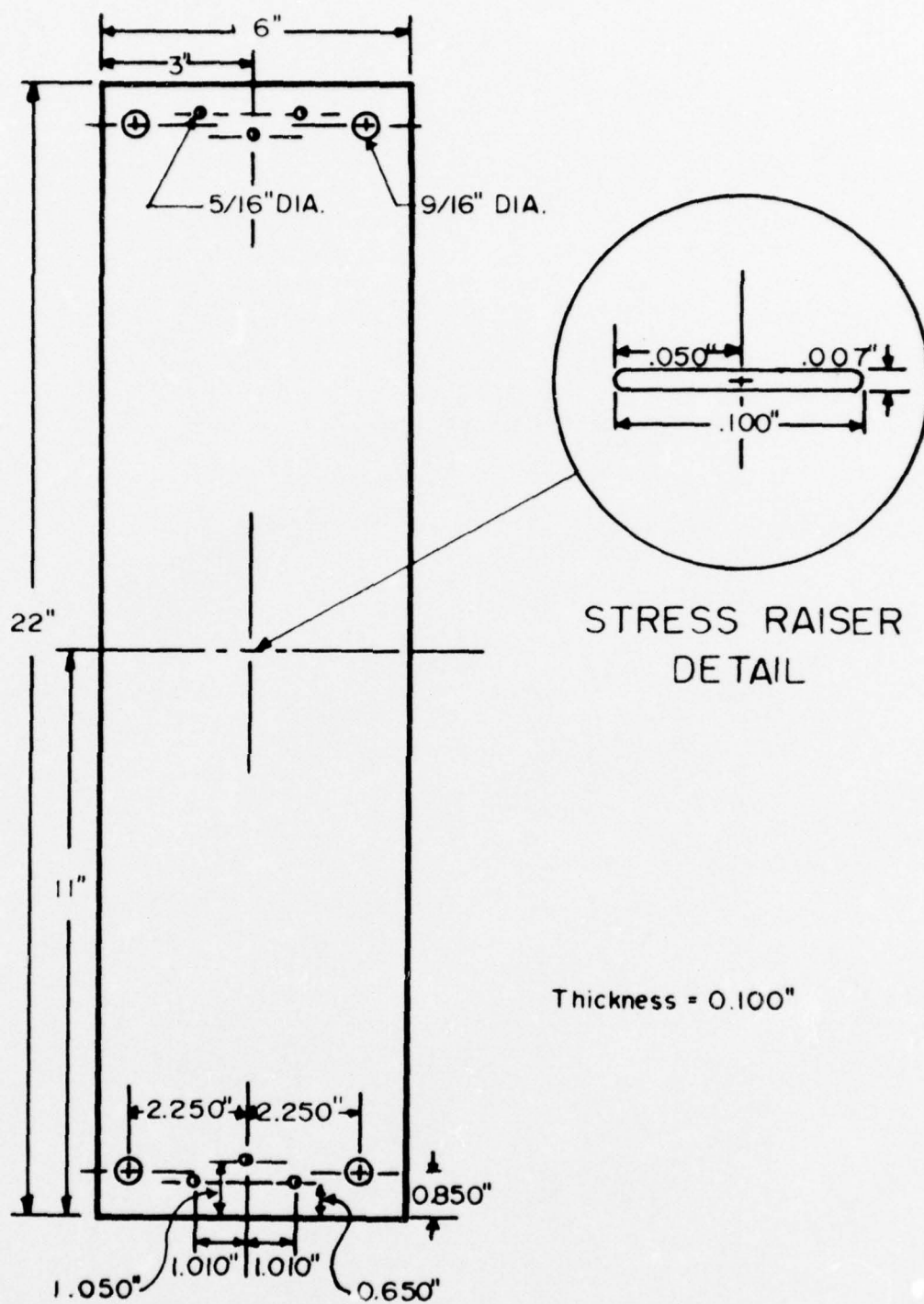
Figure 8 Center crack test specimen [24]

Table 1

TEST SPECIMEN MATERIAL PROPERTIES

2024-T3 Aluminum Alloy

	Specimens Used in This Investigation	Alzos' Specimens [5]
Yield Strength	54,400 psi	56,900 psi
Ultimate Strength	74,000 psi	69,000 psi
Percent Elongation	17.8%	14.2%

on a strip chart recorder for load verification and subsequent data reduction. All tests were run with felt lined aluminum compression guides on the specimen. These guides were utilized to mount the Elber gage and the two fringe detectors used with the interferometry measurement system. During testing an oscilloscope was used to monitor the feedback signal (load) to insure that the applied loads were not being distorted from the input sinusoid. A digital cycle counter was driven by the system feedback signal (load). Crack growth was monitored with a 100x microscope mounted on a two way traverse system. A digital resolver system on the horizontal traverse produced a digital output in the horizontal direction with a resolution of 0.001 mm. (0.0004 in). The direction of travel of the optical system was never changed during a test to eliminate any hysteresis effects in the traverse system. Both the traverse and counter outputs (crack length and number of cycles) were connected to a push button operated mechanical printer. A strobe light was triggered at the point in the load cycle where the crack tip is most clearly visible. More detailed discussions of this portion of the experimental set-up can be found in references [5] and [6].

Test Procedure

Cracks were initiated from the stress raiser, then grown a minimum of 6 mm to avoid any effects due to the stress raiser. Loads were gradually reduced during the initiation process to bring the applied stresses down to the test level.

In order to have a basis for comparison between two overload/
underload tests in the test matrix, the stress intensity factors were
held at quasi-constant values throughout each test. The stress in-
tensity factors were held quasi-constant by changing the load required
to produce a specified K value for every 5 percent increase in crack
length. This insured that actual K values were within 3 percent of the
desired values. Loads were calculated using Tada's modification to
Fedderson's formula [25] for the stress intensity factor of a center
cracked specimen. The load in pounds is:

$$P = \frac{K\,A}{\sqrt{\pi a}\ \ F(a/b)} \tag{14}$$

where

K = desired stress intensity factor (Ksi $\sqrt{in}$)

A = cross-sectional area of the specimen (in^2)

a = crack length (in)

b = specimen width (in)

f(a/b) = correction factor for specimen geometry

$$= \left[1.0 - .025\ (a/b)^2 + .06\ (a/b)^4\right]\ \sqrt{SEC\ \frac{\pi a}{2b}} \tag{15}$$

(correct to 99.9% for all a/b)

To isolate the single overload effects care was taken in each test
to establish equilibrium before the application of the overload se-
quence. Steady state conditions were achieved following in the over-
load sequence by propagating the fatigue crack over twice the diameter
of the theoretical overload plastic zone of each test at the

quasi-constant stress intensity value specified for that test. Over-load sequences were applied when the crack had propagated 5 percent past the point of the previous load shed.

All tests were run at 20 Hz except for each overload/underload sequence and each closure measurement cycle when the rate was changed to 0.02 Hz. The only interruptions during a given test were for mounting the Elber gage with the specimen at minimum load.

Discrete a versus N data points were taken by advancing the optical system by a specified increment and triggering the printer when the crack tip had grown to this incremented position.

THE ELBER GAGE

The Elber gage shown in Figure 9 provided a proven technique for measuring crack edge displacements [4]. The gage contacts the specimen through two pin points positioned such that one is located on either side of the crack. Relative motion of the crack edges causes a slight change in the geometry of the gage body. The two active strain gages are located on the most strain sensitive surfaces of the aluminum gage body and placed in opposite arms of a wheatstone bridge. Identical strain gages located on strain free surfaces of the gage body are wired into the remaining two arms of the bridge circuit to provide full temperature compensation.

The strain gages are 120 ohm gages with a gage length of 0.0625 inches and a gage factor of 2.195. An excitation voltage of 3.0 volts was applied. A BLH Signal Conditioner provided the necessary amplification. The Elber gage was found to have a working linear range from a nominal position to approximately 0.050 mm of tensile displacement. Beyond this range hysteresis effects were observed. The BLH Signal Conditioner has a maximum gain capability of 2000, which results in a full scale output of approximately 900 millivolts at a strain of 4500 $\mu\epsilon$.

The Elber gage is located on the specimen via two piano-wire beam assemblies. This configuration, shown in Figure 10, provides
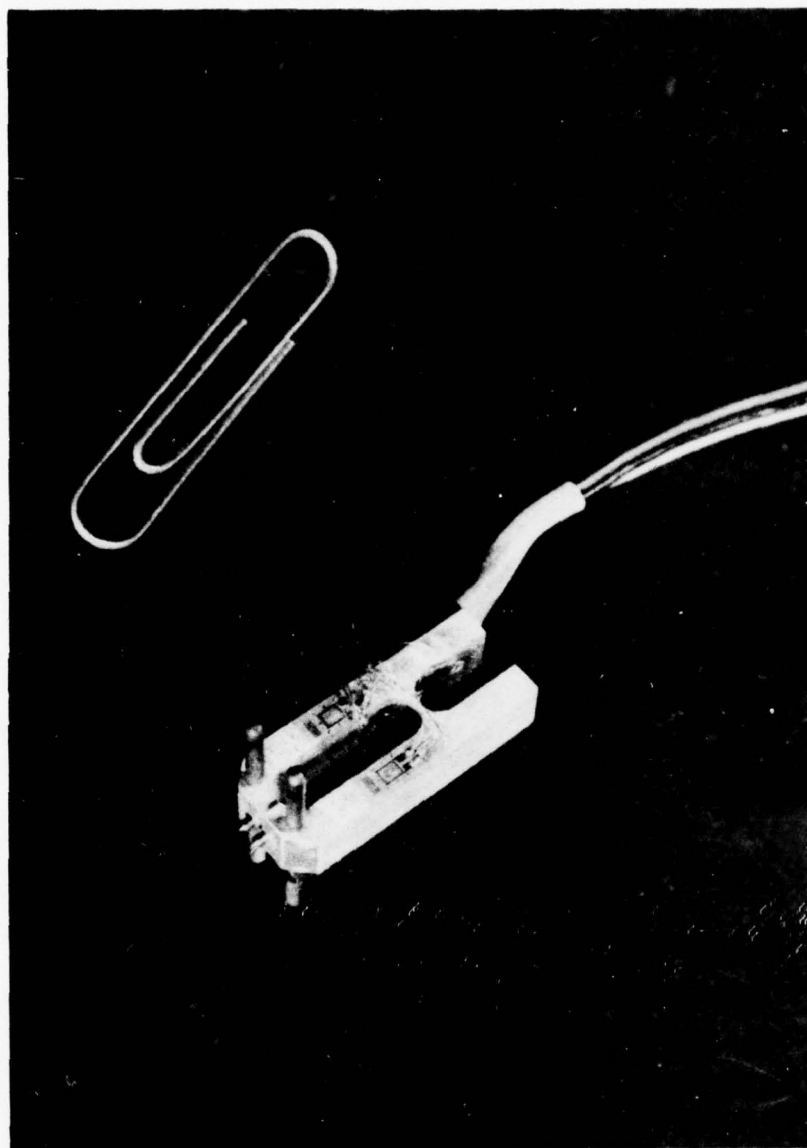
Figure 9   Elber Gage
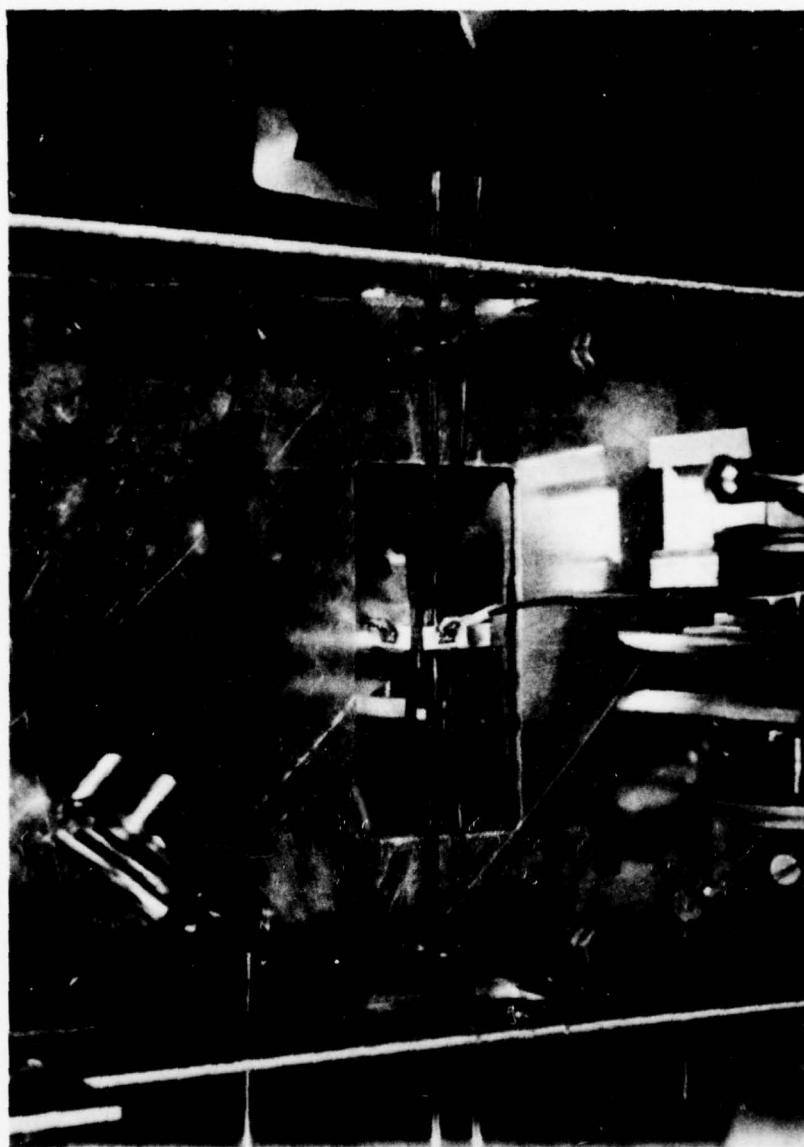
Figure 10 Elber Gage Mounted on a Test Specimen

high stiffness in bending in the plane perpendicular to the specimen and parallel to the direction of crack propagation. Torsional stiffness is provided by piano-wire clips which are attached to the compression guides. Normal force is provided by coil compression springs which act through the specimen compression guides and have provisions for adjusting spring tension. Such a configuration does not impair gage body flexure due to crack opening displacements.

Calibration

It was deemed highly desirable to calibrate the Elber gage and the optical measurement system against the same standard. Because of the very small displacements, and accuracy requirements a calibration specimen was designed. This calibration specimen was fabricated from the same heat of 2024-T3 aluminum alloy as the regular center crack panel test specimens. The material properties had already been determined experimentally.

The calibration specimen, Figure 11, has a uniform cross sectional area (1.000 in. x 0.100 in. = 0.100 in^2) which is maintained over a length of 13 inches which insures uniform strain in the region of interest. A single 350 ohm gage with a gage length of 0.125 inches and a gage factor of 2.105 was mounted to the specimen, aligned and centered with respect to the principal axis of the specimen. Bonded strain gages can repeatedly withstand elongations on the order of 10 percent of their gage length. The single gage configuration was chosen because only the strain on the front surface of the specimen was required for calibration.
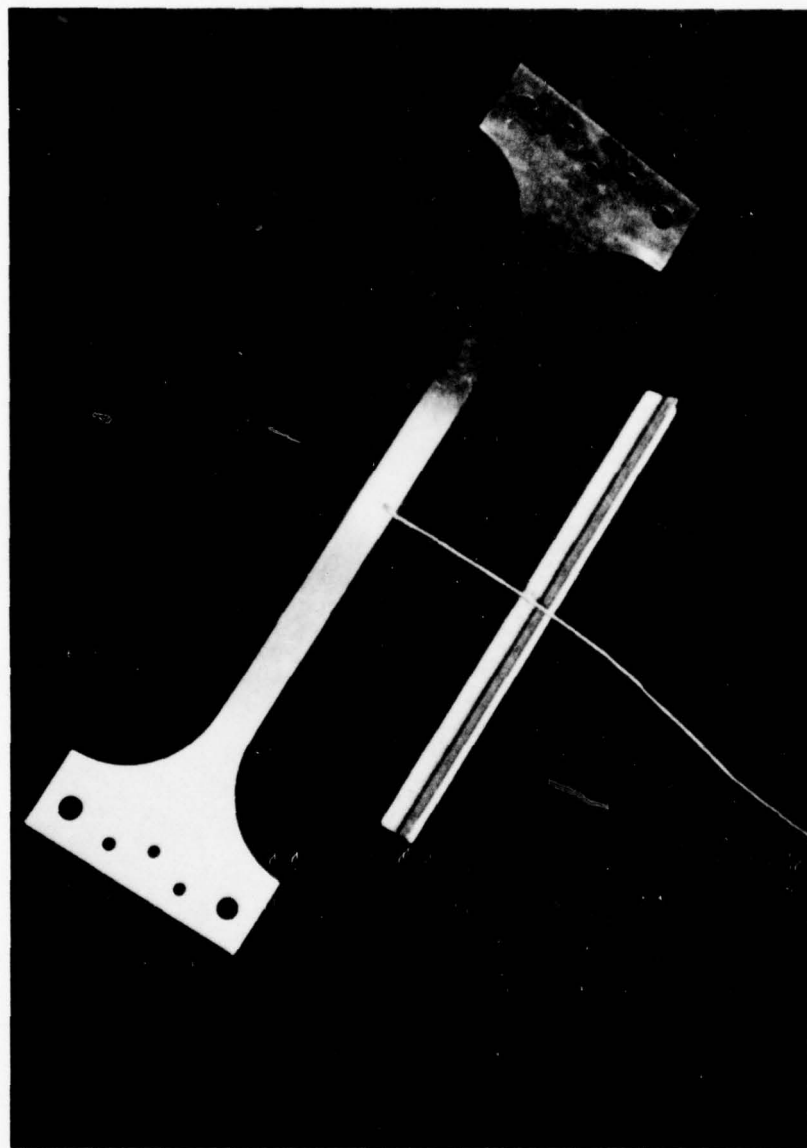
Figure 11 Calibration Specimen

The half bridge configuration of the BLH Signal Conditioner was used. Temperature compensation was provided by a three wire hook-up. The strain gage was selected to have thermal expansion properties similar to the specimen material. A 351 ohm (measured) resistor was used in the compensating arm of the half bridge.

The absolute amount of strain experienced by the tensile calibration specimen was inferred by shunting an additional resistor of known value into the active arm of the half bridge. Zero strain was defined by zeroing the BLH amplifier with the calibration specimen attached only to the upper fixture of the test machine. Then by shunting the calibration resistor across the compensating arm of the bridge a strain was simulated electrically, allowing the amplifier gain to be adjusted to the desired full scale output.

The maximum amount of elastic strain, $\varepsilon_{elastic}$, that the calibration specimen could repeatedly tolerate was found from the material properties as follows:

$$\varepsilon_{elastic} = \frac{\sigma_{ys}}{E} \tag{16}$$

where

E = Young's modulus

The maximum strain during calibration was limited to 4500, $\mu\varepsilon$, below the elastic limit of the material. A calibration resistor of 38.2 K ohm (measured) was used to give a calibration strain of approximately 90 percent of the full scale strain. The final equation for the simulated strain is:

$$\varepsilon_{CAL} = \left[\frac{R_{COMP}}{R_{COMP} + R_{CAL}} \right] \cdot \left[\frac{1}{\text{Gage Factor}} \right] \tag{17}$$

where

ε_{CAL} = electrically simulated strain

R_{COMP} = resistance in the compensating arm of the bridge network

R_{CAL} = resistance of the calibration resistor.

The amplifier gain was adjusted to produce a full scale output of 900 mv which corresponded to a strain of 4500 $\mu\varepsilon$.

The gage length of the unstressed Elber gage was found to be 6.93×10^{-2} in. This was determined using a 10x objective in conjunction with a 10x graduated retical eyepiece. The Elber gage was also calibrated over a range of $4.500 \times 10^{-3} \frac{in}{in}$ strain or 3.118×10^{-4} in. displacement. Preliminary investigation indicated that this was well within the linear range of the gage. During installation of the gage on the specimen a piece of shim stock (0.020 in) inserted between the gage body surfaces was used to produce a repeatable gage length which was approximately 0.068 in.

DEVELOPMENT OF THE INTERFEROMETRY SYSTEM
FOR DISPLACEMENT MEASUREMENT

Background

Recent experiments have shown that laser interferometry can be utilized for very accurate measurement of fatigue crack closure in structural metals [18,19,20,21,22]. In this study these techniques are applied to dynamic load conditions.

Young's double slit experiment demonstrates that the Fraunhafer diffraction of light from two slits produces an interference fringe pattern [26]. The spacing of these fringes is a function of the separation of the slits according to the formula:

$$m = \frac{d}{\lambda} \sin \theta \quad m = 0,1,2,\ldots \text{(maxima)} \tag{18}$$

where

    d = slit separation

    λ = wavelength of light

    θ = angle between the normal to the plane containing
         the slits and the line from the center of the
         slits to the point of observation, P

    m = order of the fringe.

The difference in optical path lengths from the upper and lower slits to the fixed observation point, P, is represented by ΔR. It can be seen from Figure 12 that when

$$\Delta R = d \sin \theta = m\lambda \quad m = 0,1,2,\ldots \tag{19}$$
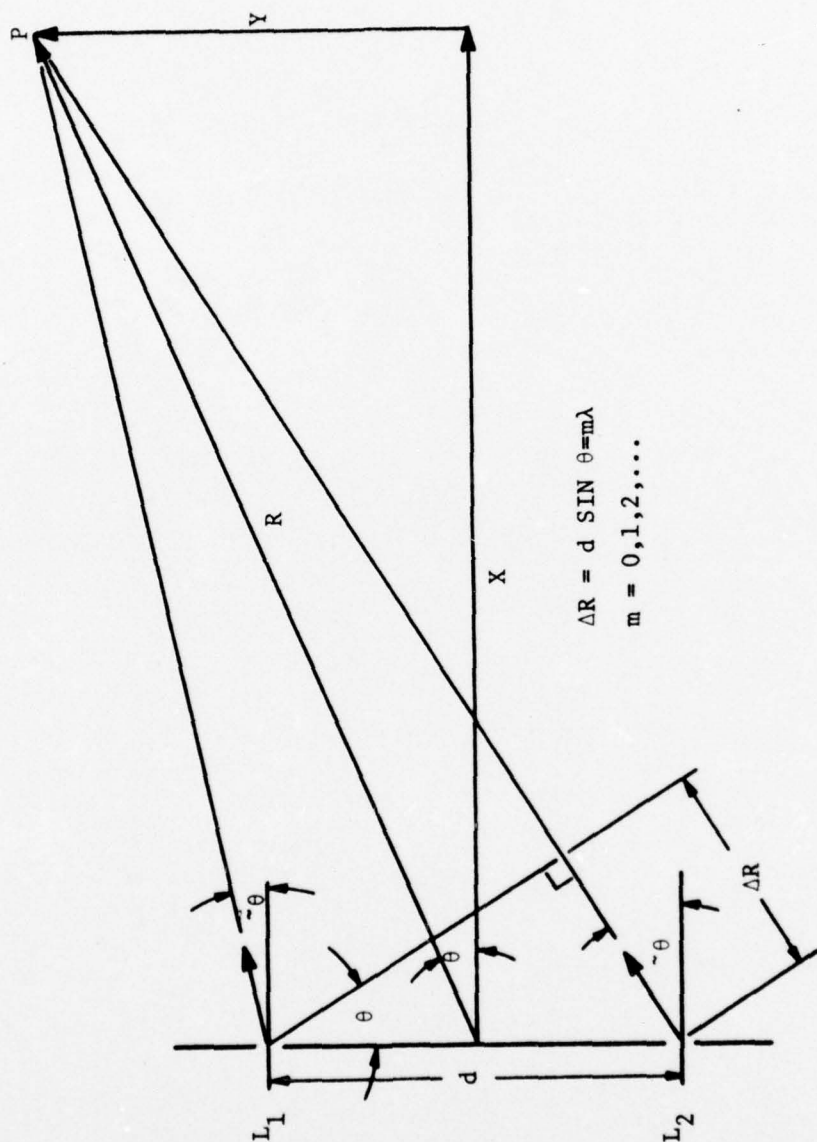
Figure 12 Geometry for Analyzing Interference
in the Case of a Double Slit

$\Delta R = d \, SIN \, \theta = m\lambda$

$m = 0,1,2,\ldots$

that the intensity is a maximum at point P. This assumes that d is small compared R, the optical path to the detection point P from a point midway between the two slits.

This same equation will hold when d is now the distance between the two indentations which reflect the incoming laser beam at some angle (70° in this system).

If one observes the fringe pattern from a fixed observation position, defined by an angle Θ_o, while the grooves move relative to each other, the fringes move past this position, and the relation between displacement and fringe motion, δm, is

$$\delta d = \frac{\lambda}{\sin \Theta_o} \delta m \qquad (20)$$

where

δd = change in displacement between the indentations

Θ_o = angle measured from a plane perpendicular to a plane normal to the specimen and parallel to the crack, to the receiving aperature

δm = the number of fringes or fractions thereof passing the observation point.

Figure 13 shows the details of the double groove case.

The sensitivity of the displacement measurement is not directly related to the original distance between the grooves. However, the angular spacing of the fringes, $\delta\Theta$, is given by

$$\delta\Theta = \frac{\lambda}{d \cos \Theta} \qquad (21)$$

where

$\delta\Theta$ = angular fringe spacing

Thus if the grooves are close together the fringes are far apart and easier to resolve.
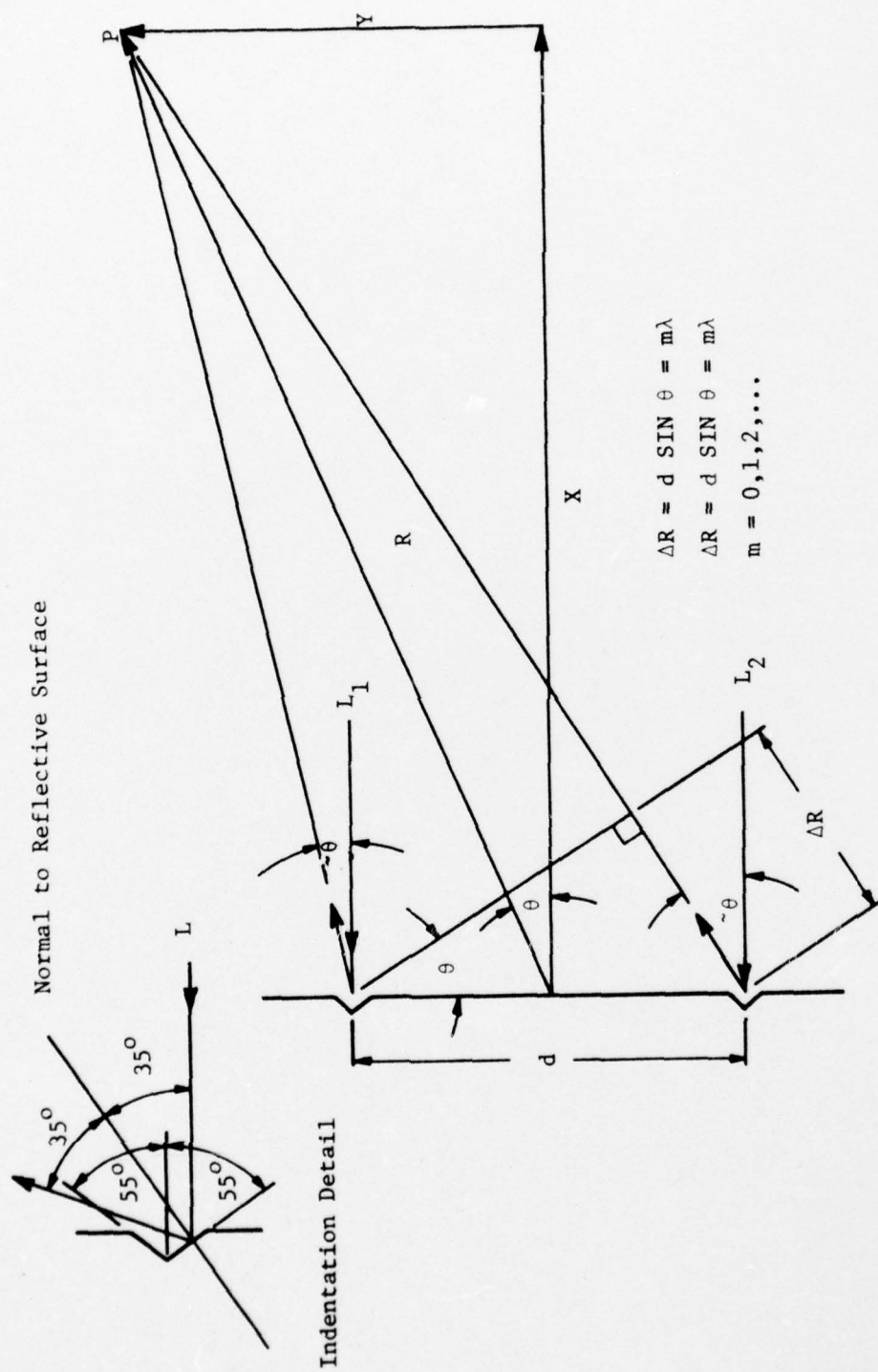
Figure 13   Geometry for Analyzing Reflected Interference in the Case of Two Indentations

If the two grooves of Figure 13 move apart, the fringes move toward that incident laser beam. This is explained by Equation 21 which shows that as d increases θ must decrease. It is therefore convenient to define fringe motion toward the incident beam as positive; motion away as negative. Of course, fringe motion occurs with any rigid body motion of the sample. However, if the two pattern motions are averaged using the above sign convention, rigid displacement in the surface plane perpendicular to the indentations and rotation about a horizontal plane parallel to the indentations will be averaged out. Other rigid body motions can lead to errors, which will be discussed in a separate section.

Application

A wedge shaped diamond tool was employed to make the indentations in the sample. The diamond has a working edge of 0.100 inches with an included angle of 110°. When this tool is pressed into the sample it produces an indentation whose sloping sides act to concentrate the diffracted light at an angle of $\pm 70^{O}$ from the normal to the specimen when the laser beam is perpendicularly incident.

The diamond tool is mounted in a brass fixture which threads into a microscope turret and is secured by a lock ring. The other aperature of the turret has a microscope objective (10x or 20x) with a cross hair which is used to position the diamond relative to the crack tip prior to making the first mark. Precise alignment of the diamond with the sample surface is accomplished through eight set screws securing the tool in the holding fixture. This arrangement is shown in Figure 14.
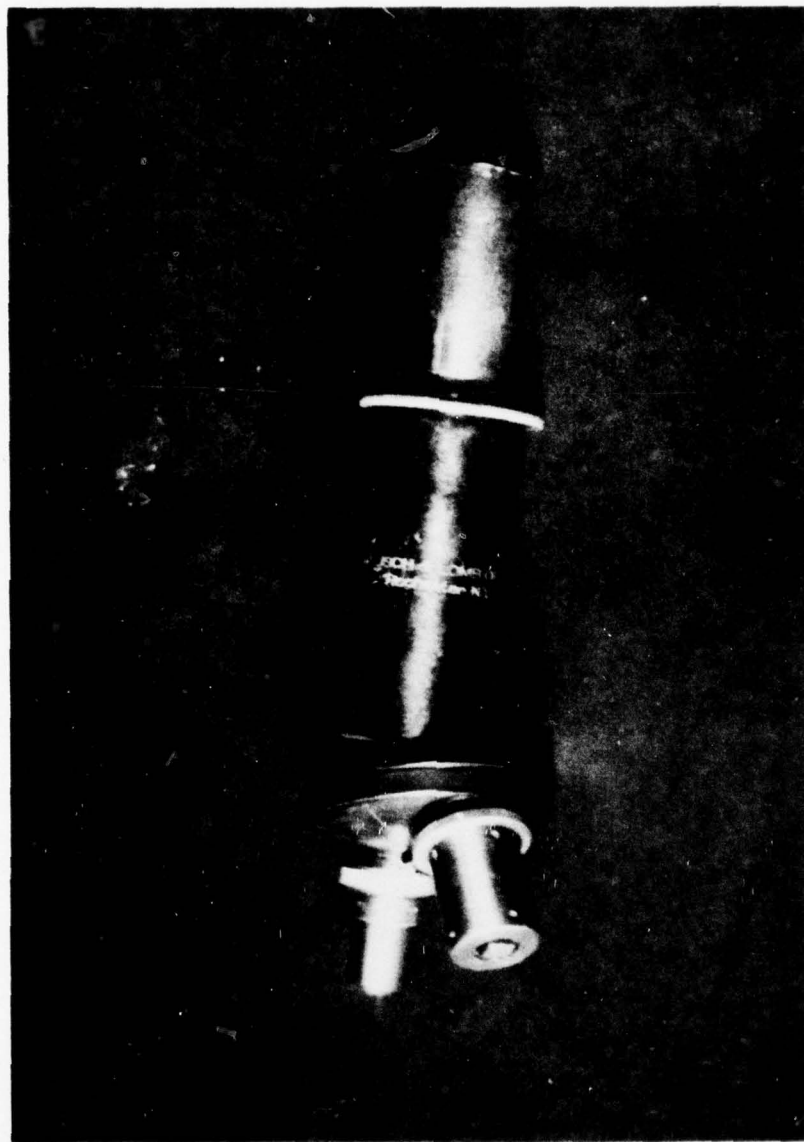
Figure 14 Diamond Tool and Microscope

Two marks are made with this tool, one above and one below the fatigue crack. Proper spacing between the marks was accomplished by first positioning the cross hair on the crack tip then rotating the turret bringing the diamond tool into position. Light pressure was applied by hand to make the indentation. The cross hair was then replaced by a graduated retical which allowed the vertical traverse to be moved down a distance of 250 microns. The turret was again rotated allowing the second mark to be made.

For the interferometric measurement system monochromatic coherent light is obtained from a Spectra Physics 123 He-Ne laser which operates at a wavelength of 632.8 nm. The laser is mounted and adjusted so that the plane of the beam is perpendicular to the plane of the sample. A diverging lens is used to expand the laser beam such that the intensity is approximately uniform over the specimens vertical range of motion. The beam is reflected through a cylindrical lens obliquely onto the surface of the sample. This cylindrical lens produces a narrow width beam perpendicular to the indentations. The light is then reflected from both surfaces of each mark producing a set of interference fringes at each receiving aperature. Cylindrical lenses are used to focus the fringes at each receiving aperature.

Phototransistors* are used as detectors. Light from the fringes is conducted to the detectors by fiber optic cables. The receiving end of each cable is rigidly attached to the compression guides and

---

* Darlington Model #2N5777.

oriented to detect the reflected fringes through a narrow slit aperature. These slits are adjusted so that the fringes are parallel to slit aperatures on the ends of the fiber optics cables. An isometric drawing of the system is presented in Figure 15.

As a load is applied to the specimen the marks move apart resulting in movement of the fringes past the detection slits. This results in a change in the voltage output of the phototransistors. This voltage is recorded along with the load cell voltage on a strip chart recorder.

Calibration of the optics system was accomplished by staticly simulating several complete cycles. This was done by moving a slit across the fringes using a micrometer stand. This produces a cosine squared wave for the voltage signal output. By adjusting minimum and maximum voltage levels this wave form can be related to the actual test signal. Resolution is a function of slit position relative to the cosine squared wave peak. Maximum resolution occurs while operating in the linear range of the characteristic curve. An overall view of the interferometric displacement measurement system appears in Figure 16.

Measurement Procedure

The following procedure was employed in making displacement measurements in the vicinity of the crack tip with the optical system.

Utilizing the microscope with a 20x objective and the diamond tool in opposite sides of the turret and illuminating the sample

47

1. Laser
2. Diverging lens
3. Mirror
4. Cylindrical lens
5. Specimen
6. Cylindrical collection lens
7. Detector with slit
8. Fiber optics cable
9. Phototransistor in case
10. Compression guides
11. EDM slot
12. Indentations
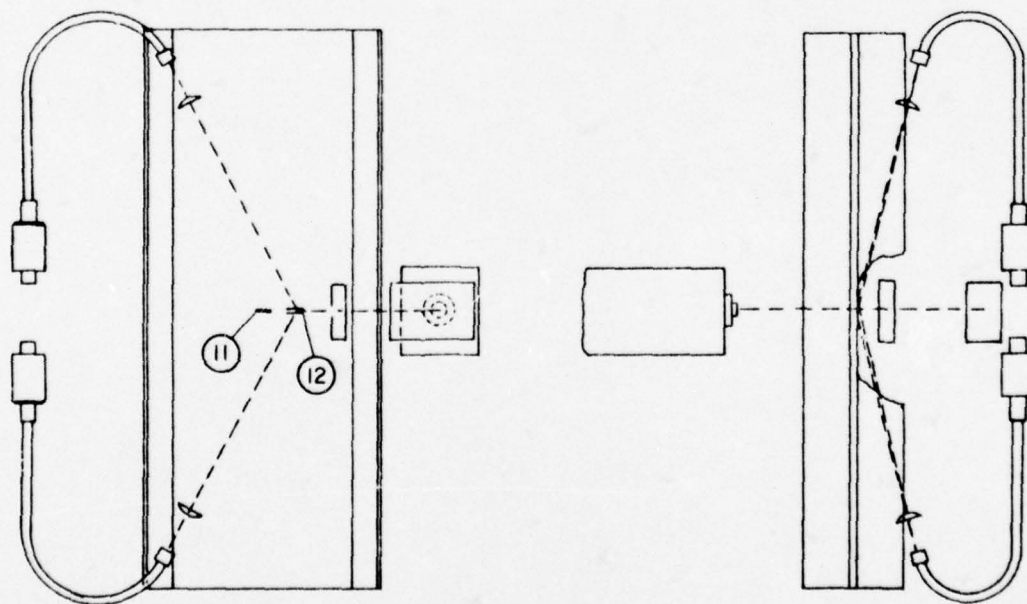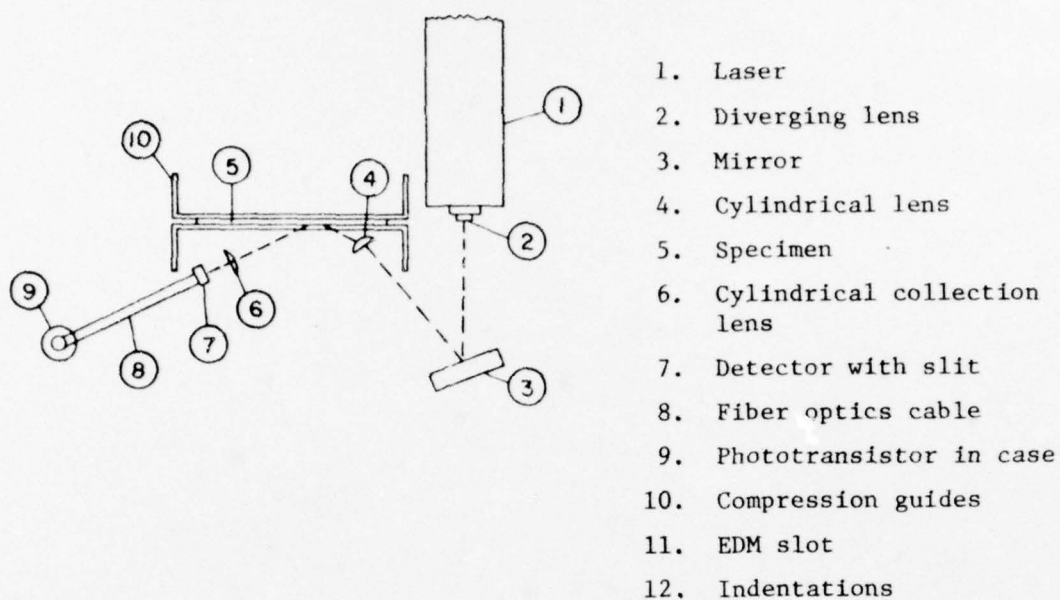
Figure 15   Isometric Drawing of the Interferometry
Measurement System
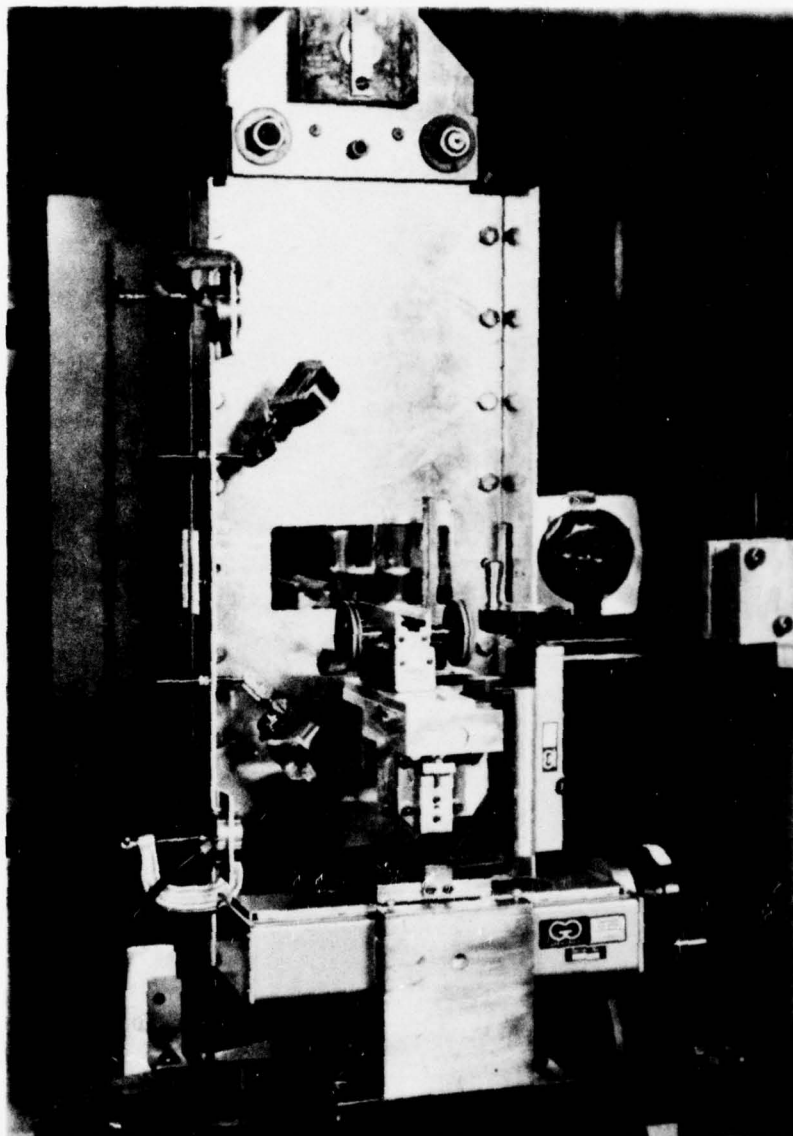
Figure 16   Interferometry Measurement System

surface with a high intensity light, parallel marks, spaced equi-
distant from the crack, were made on the sample. For a given test these
marks were spaced approximately 250 microns apart while the specimen
was at minimum load. Actual mark separation was measured optically
using a graduated retical in the eyepiece. The marks were 0.100 in.
long and are placed such that they were approximately 0.02 in. beyond
the crack tip. This allowed measurements up to and slightly ahead of
the crack tip.

The laser is oriented so that the beam is in a plane perpendicular
to the surface of the specimen. Further adjustment of the laser and
the mirror about their respective vertical axes insures that the
center of the beam strikes the point at which the measurement will
be made, and that the fringes are in the proper detection area. The
orientation of the mirror about a horizontal axis is adjusted to
maximize the intensity of the fringe pattern. The cylindrical lens
is positioned and adjusted to yield a narrow, vertical, focused band
of light across the measurement spot.

The detector receiving lenses are adjusted such that the fringes
are perpendicular to the cylindrical lens axis and are focused in the
area of the fiber optics receivers. These receivers are oriented
with their slits parallel to the fringes, then translated to the
brightest fringe. This is accomplished by watching the detector
outputs on an oscilloscope while adjusting their position. The slit
is then positioned roughly midway between the minimum and maximum of
that fringe. Starting in this linear range gives maximum sensitivity.

The detectors are then connected to a strip chart recorder and the output is monitored through several load cycles (0.02 Hz) to determine if the desired information is being received. A visual check is made at the slits to assure that the fringe motions are in the proper directions. The reasons for this check are explained in the next section.

The output of both phototransistors are recorded along with the load signal. This allows determination of displacement at any point in the load cycle. This displacement is determined by averaging the number, and fractions thereof, of fringes which move across the detector slits. This technique cancels the effects of any rigid body specimen rotations about a horizontal axis parallel to the crack.

The Effects of Rigid Body Motions

The interferometry based displacement measuring system displayed sensitivity to various rigid body motions. An explanation of these motions and their effects is as follows:

1) Rotation around a horizontal axis of the specimen causes equal and opposite fringe shifts at the upper and lower detectors. This effect can be compensated for by averaging the upper and lower fringe shifts. The geometry and relations needed to justify this technique are presented in Figure 17.

2) A translation along a horizontal axis normal to the plane of the specimen (drumming) results in a fringe shift equal to the amount of movement of both the upper
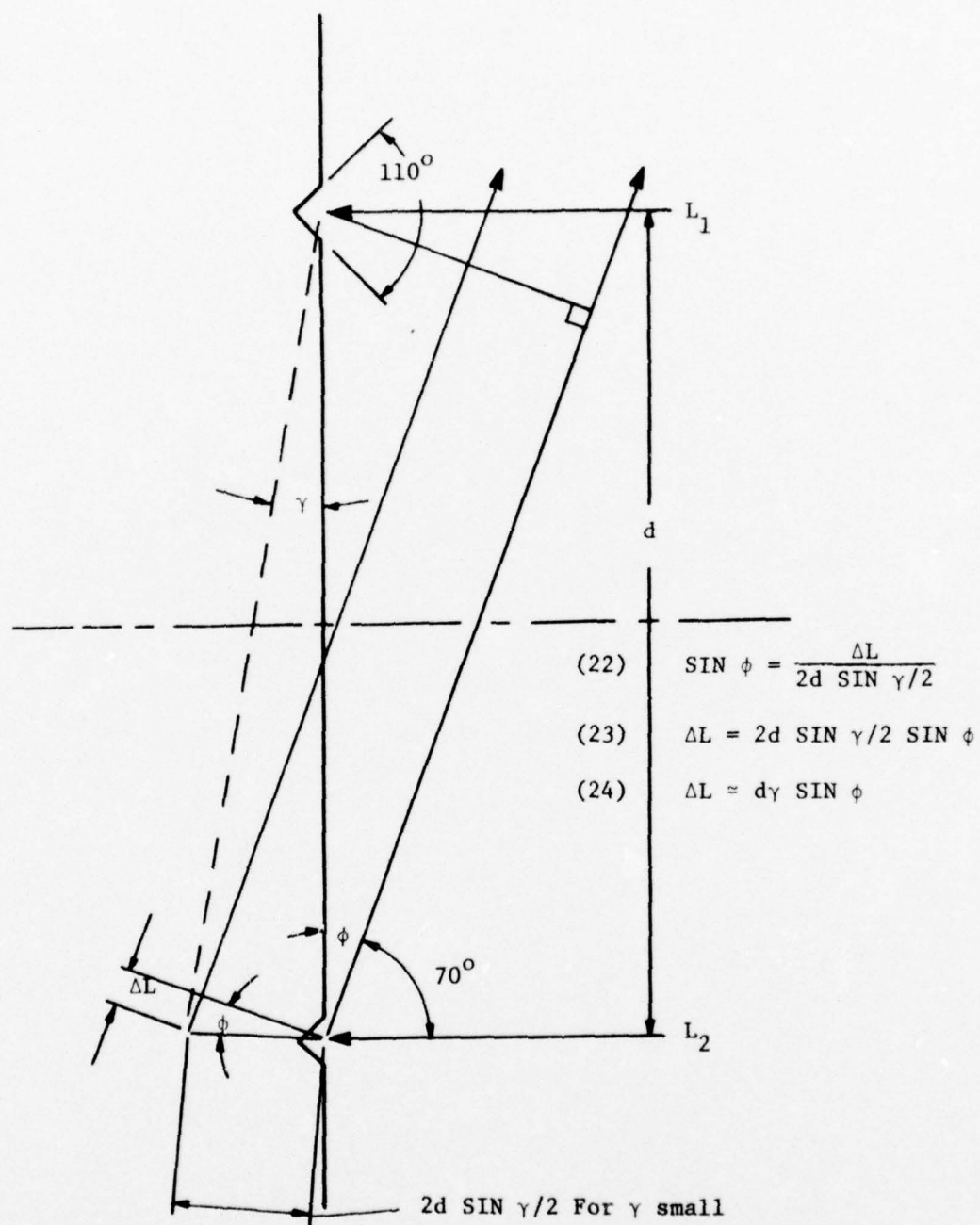
Figure 17 Geometry for Analyzing the Effect of Rotation About A Horizontal Axis Parallel to the Plane of the Specimen

and lower fringe pattern. If this movement is small compared to the fringe width at the detectors the effect will be negligible. Due to our optical geometry (refer to Figure 15) however, a movement of this nature changes the position at which the measurement is being made relative to the crack tip. This effect was experimentally determined to be quite small. When the laser was oriented such that the incident beam was normal to the plane of the specimen no detectable change in the displacement measurement was noted.

3) A rotation about a vertical axis parallel to the plane of the specimen results in a sideways movement of the fringes across the cylindrical lenses. If this movement is large enough a portion of the fringe pattern is lost. This can result in an apparent fringe shift. An attempt was made to minimize this effect through the use of cylindrical collecting lenses in front of the detectors.

4) Translation of the entire specimen along the vertical axis due to specimen loading will cause the indentations to move relative to the incident laser beam. This results in an intensity change of the fringes. Again this would appear as an apparent fringe shift. The diverging lens immediately in front of the laser should have minimized this effect by spreading the beam to produce more uniform intensity vertically across the measuring area.

5) Rotation about a horizontal axis normal to the plane of
the specimen has the effect of changing the indentation
spacing. This results in an apparent fringe shift which
would be indistinguishable from crack opening. Measure-
ments made with dial indicators did not reveal any de-
tectable rotation of this type in the system.

6) A pure horizontal translation in the plane of the specimen
effectively changes the position at which the measurement
is being made. Any of these effects would be magnified
by the indentations not being parallel. Nonuniform in-
dentation depth can change the fringe intensity if one of
these movements occurs.

DATA REDUCTION

Determination of Crack Open Load From Elber Gage Data

A two channel strip chart recorder was used to monitor the
Elber gage output voltage and the load cell voltage, both as functions
of time. During data collection the cycle frequency was 0.02 Hz. A
ramp wave form was selected for the input load so that the applied
load would be a linear function of time. For each test several con-
secutive cycles were observed at chart speeds of 5 mm/sec and 25 mm/sec.

The internal filtering of the BLH Signal Conditioner which was
used to amplify the Elber gage output voltage, was employed. This
was necessary to eliminate unwanted high frequency noise. Accompanying
this filtering was a phase lag of approximately 7.0 degrees. This
phase was constant for all tests and was compensated for in subsequent
data reduction. This is illustrated in Figure 18.

By reducing the load and Elber gage signal versus time a load
versus deflection or strain curve can be constructed exhibiting the
characteristic hysteresis. A typical curve is shown in Figure 19.
Elber defined P_{OP} by utilizing the initial slope of the unloading
portion of such a curve. The point at which a line parallel to this
initial unloading slope is tangent to the loading segment of the
curve defines P_{OP-25}.
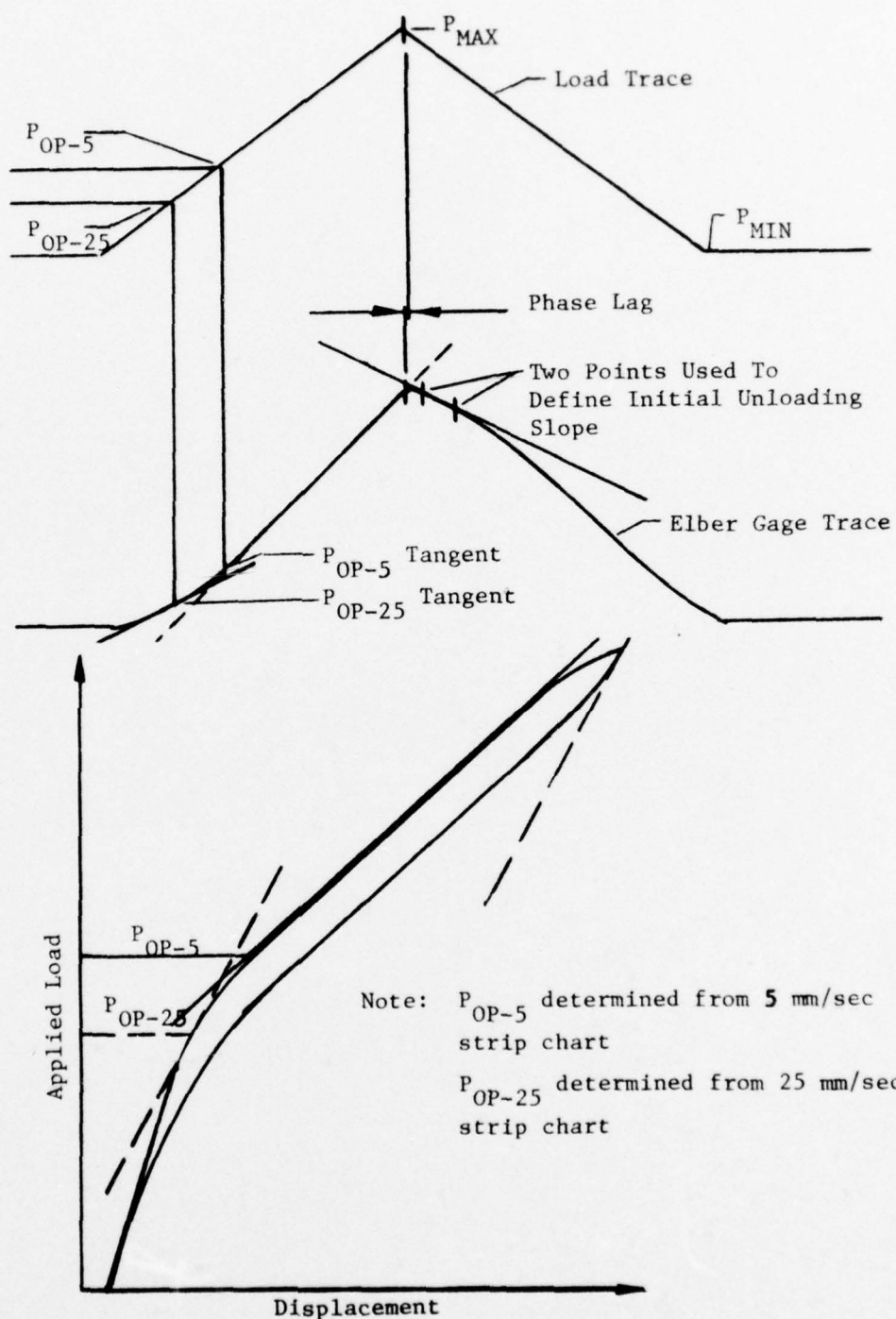
Figure 18 Typical Load and Elber Gage Trace Exhibiting Phase Lag and Showing the Determination of P_{OP-5} and P_{OP-25}
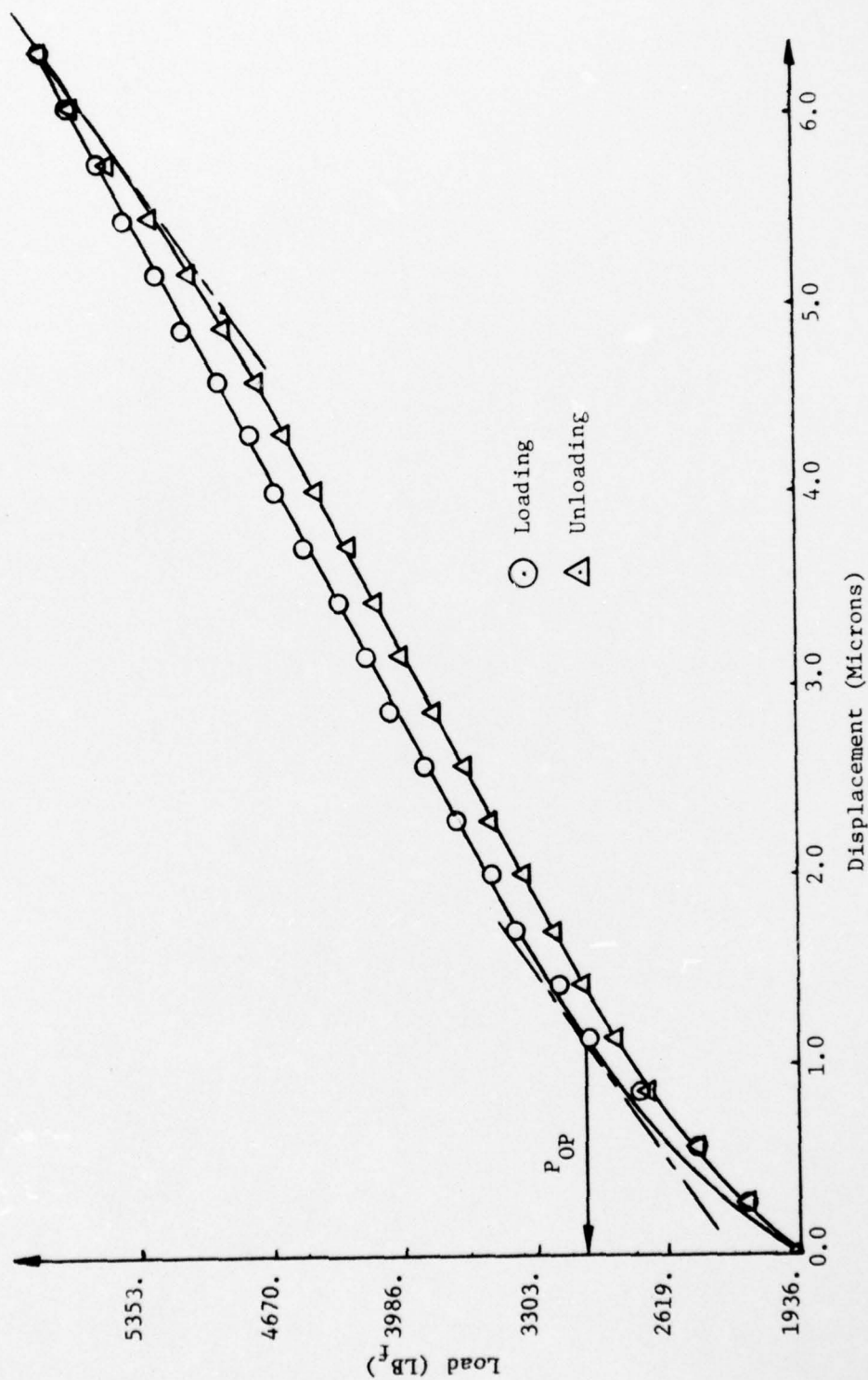
Figure 19 Load vs. Displacement Curve Plotted From Elber Gage Data

Working from the 25 mm/sec traces the slope could best be de-
fined by two points from the Elber gage output fixed distances from
the peak signal. The two points defining this slope were chosen
10 and 36 divisions beyond the peak. Data reduction was performed
directly on the traces by using the negative of this slope and finding
the point of tangency on the loading segment of the Elber gage signal.
This tangency point gives the time corresponding to P_{OP-25} and from
the ramp load curve the value of P_{OP} was determined after accounting
for phase lag. This procedure is illustrated in Figure 18.

Nonlinearities in the Elber gage output are more readily observed
in the traces made at a chart speed of 5 mm/sec. The loading portion
of these curves characteristicly exhibit a nonlinear segment followed
by a linear region. As the peak load is approached the curve is
again nonlinear. From the load displacement relationship the lower
transition from nonlinear to the linear portion of the trace represents
the upper value of P_{OP}. Drawing a straight line on the loading seg-
ment of the Elber gage output coincident with the linear portion
allows determination of this transition point and subsequently of
P_{OP-5}. It is realized that these are somewhat arbitrary methods for
determining P_{OP} however, they are based on the definitions of the
opening load as defined by Elber and on his technique. Maximum
sensitivities were used on both strip chart channels in an attempt
to minimize the inaccuracies inherent in these techniques.

Determination of Crack Opening Load From Interferometry Data

Data collected from the laser interferometry measurements were reduced by two slightly different techniques depending on the total amount of displacement measured.

When measurements were made very near to the crack tip the response was generally less than one complete fringe shift. See Figure 20. A preliminary test was performed prior to attempting any measurement. Several samples of the minimum and maximum photo-transistor output were recorded on the strip chart by moving several fringes across the detector slit. While the individual maximum and minimum levels vary slightly as a function of fringe intensity, the difference between the levels remains essentially constant over the number of fringe shifts of interest.

Upper and lower responses are noted at selected load increments. This allows determination of fractional fringe movements with the degree of accuracy being limited by the DC magnitude and amplification of the difference in the minimum and maximum outputs of each photo-transistor. Once reduced, the upper and lower fringe movements are averaged to eliminate the effect of rigid body rotation about an axis parallel to the crack. For small discrepancies in the peak to peak amplitude of cycles from a single detector due to intensity changes in the fringe pattern two approaches are used: 1) the average of the maximum and minimum level of all the cycles is used or, 2) with larger variations each cycle is normalized with respect to its mean level.

When measuring more than 1.25 mm behind the crack tip, ten or more complete cycles, (or fringe shifts) generally occured. This situation is shown in Figure 20. Rather than divisions, cycles and fractions thereof are noted at selected load intervals. Discrepancies in peak to peak amplitude are more likely to occur when measuring larger displacements. Compensating as explained above reduces confidence in the accuracy of the magnitude of an absolute displacement or strain value however, this does not affect the determination of P_{OP}.

The load is plotted as a function of fringe shift, yielding a hysteresis curve quite similar to that plotted from Elber gage data. A best fit curve is drawn through the lower 75% of the loading curve. The slope of the unloading curve is determined by a straight line drawn through points clustered between 80 and 90 percent of P_{MAX}. The point where this slope is tangent to the best fit loading curve gives P_{OP}. This technique is functionally equivalent to the Elber gage data reduction. A typical load versus displacement curve showing the determination of P_{OP} is presented in Figure 21.
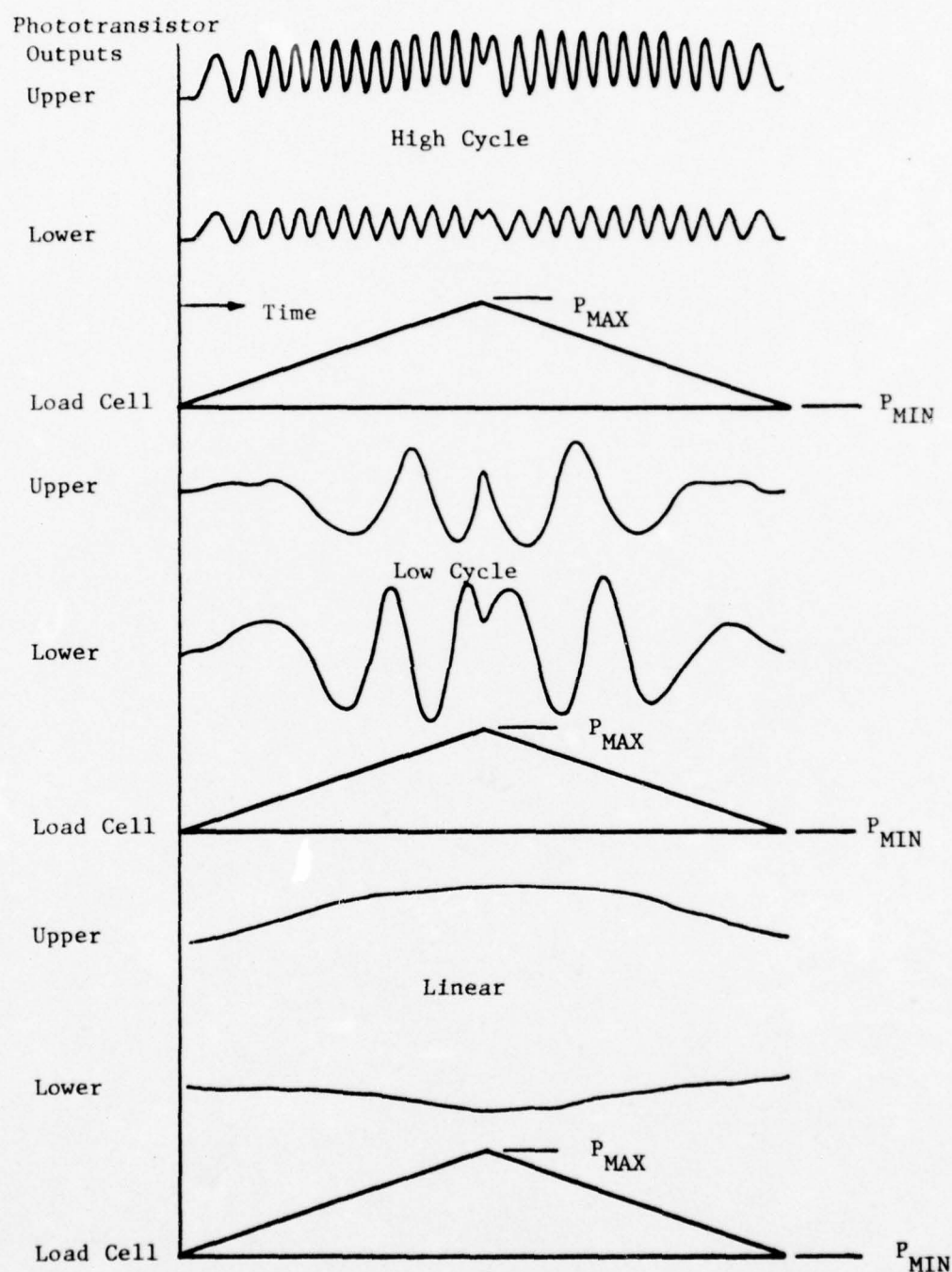
Figure 20   Typical Load and Interferometry Traces for Measurements
At Various Distances Behind the Crack Tip

61
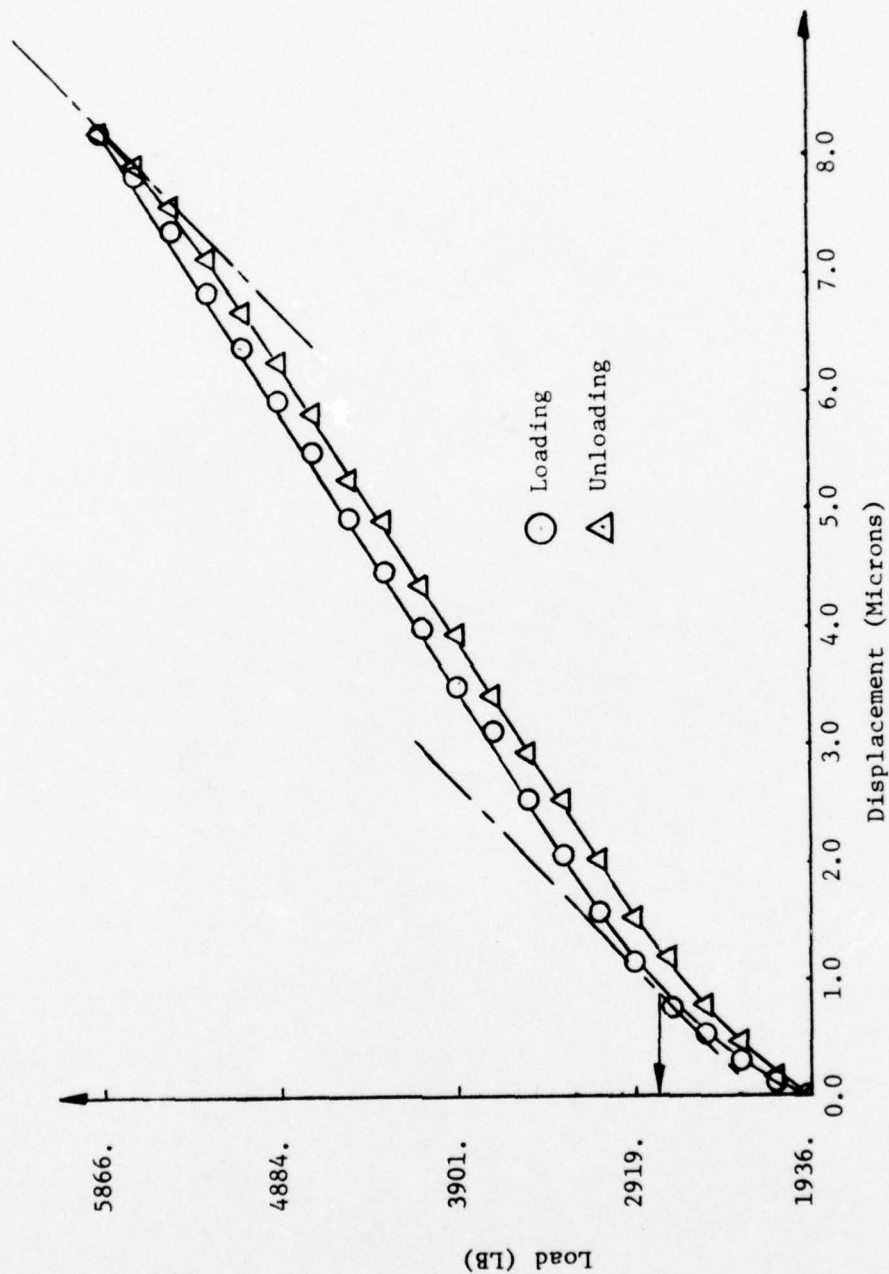
Figure 21 Load vs. Displacement Curve Plotted From Interferometry Data

TEST RESULTS AND OBSERVATIONS

Many comparisons will be made to the results obtained by Alzos
[5] and to aid in this his results relevant to this investigation
may be found in Appendices A and B. Several important differences
in the tests should be noted. While the material in each case was
2024-T3 aluminum alloy, the specimens used in this study came from
a different heat and therefore have slightly different material pro-
perties. Because of the frequent crack opening displacement measure-
ments it was not feasible to conduct the tests in a desiccated
environment. This effect seems to be one of considerable significance
[12].

All tests were run with felt lined, light weight, compression
guides attached to the specimen. This was necessary because the
compression guides were used to support the mounting structure for
the Elber gage as well as providing attachment points for collection
lenses and the photo detectors used in the interferometry based
displacement measuring system.

a versus N data was differentiated by way of a fifteen point
moveable strip method while Alzos fit a series of cubic spline functions
to his data which allowed an exact analytic derivative to be taken
and subsequently evaluated. While his approach has some merit it
has the significant effect of artificially smoothing any results it

generates. Actual fatigue crack propagation appears to be more erratic and discontinuous in nature. Results presented in the Appendix B have been obtained using the 15 point moveable strip technique of differentiation.

Finally because single cycle operation was frequently required a different function generator was employed. Thus the overload/underload procedure used in this study was slightly different because the sequence was applied from the minimum load rather than the mean load of the cycle.

Constant Stress Amplitude Test Results

Sixteen constant amplitude tests were conducted at R_F levels of 0.01, 0.11, 0.22, and 0.33. At each of these stress ratio values four values of ΔK were used as test starting points. Crack length and the corresponding number of cycles were recorded over approximaely a 0.500 mm range of a. The specimen was then single cycled at 0.02 Hz using a triangular wave form as Elber gage and then interferometry data were collected. Analysis of the a vs. N data by plotting a vs. N and subsequently log da/dN versus log ΔK_{EFF} confirmed that the test conditions under which K_{OP} measurements had been obtained were representative. Displacement (or strain) versus applied load data from the two methods was subsequently reduced allowing direct comparison of K_{OP} values. Figure 22 shows da/dN versus ΔK_{EFF} for each individual R_F level. Finally da/dN versus ΔK_{EFF} curves for all the data were plotted in Figure 23 their shape compared favorably with the more extensive constant amplitude data taken by Alzos [5], although some layering was noticeable. His results appear in Figure A-1 of Appendix A.
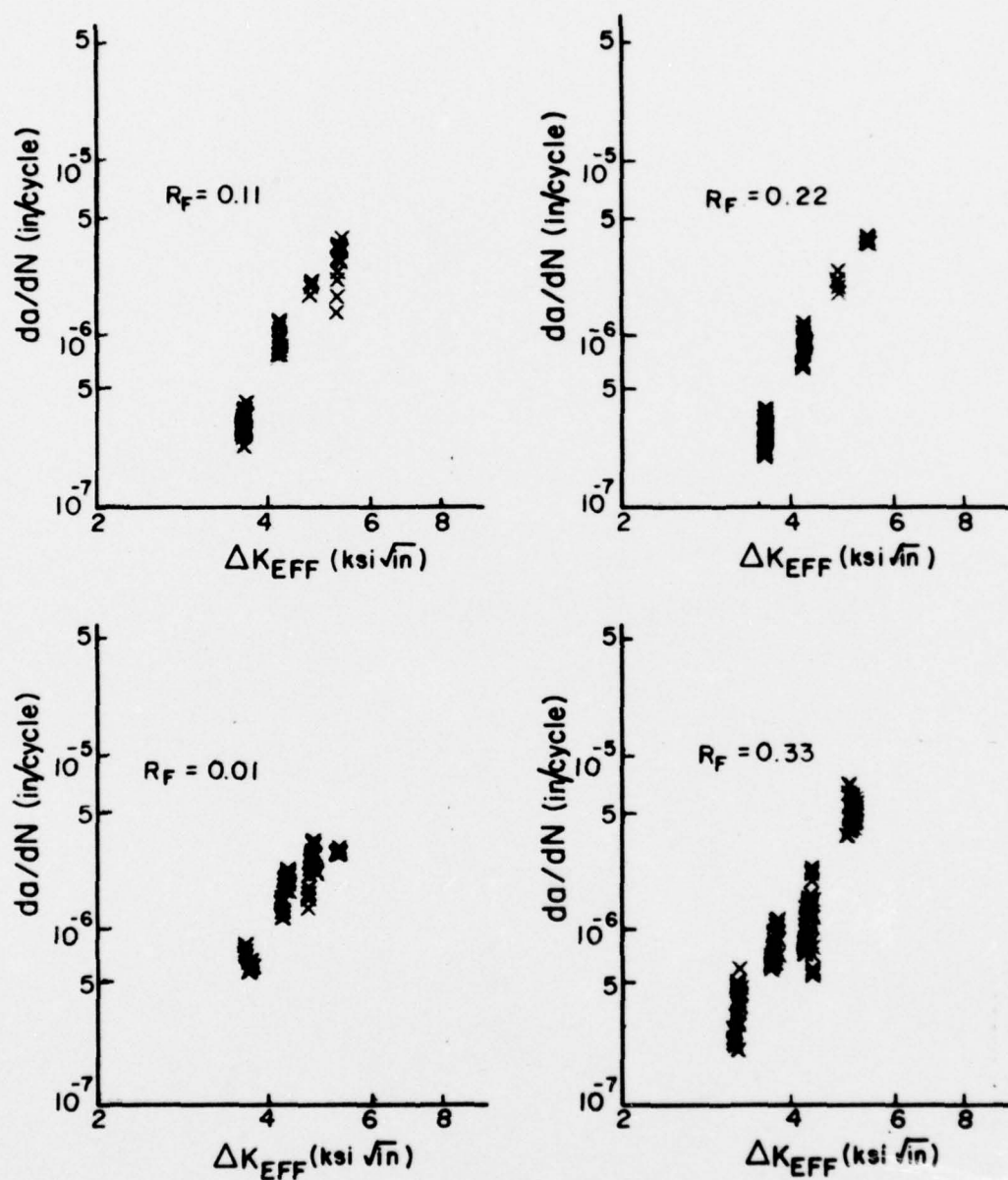
Figure 22 da/dN vs. ΔK_{EFF} for Each R_F Level
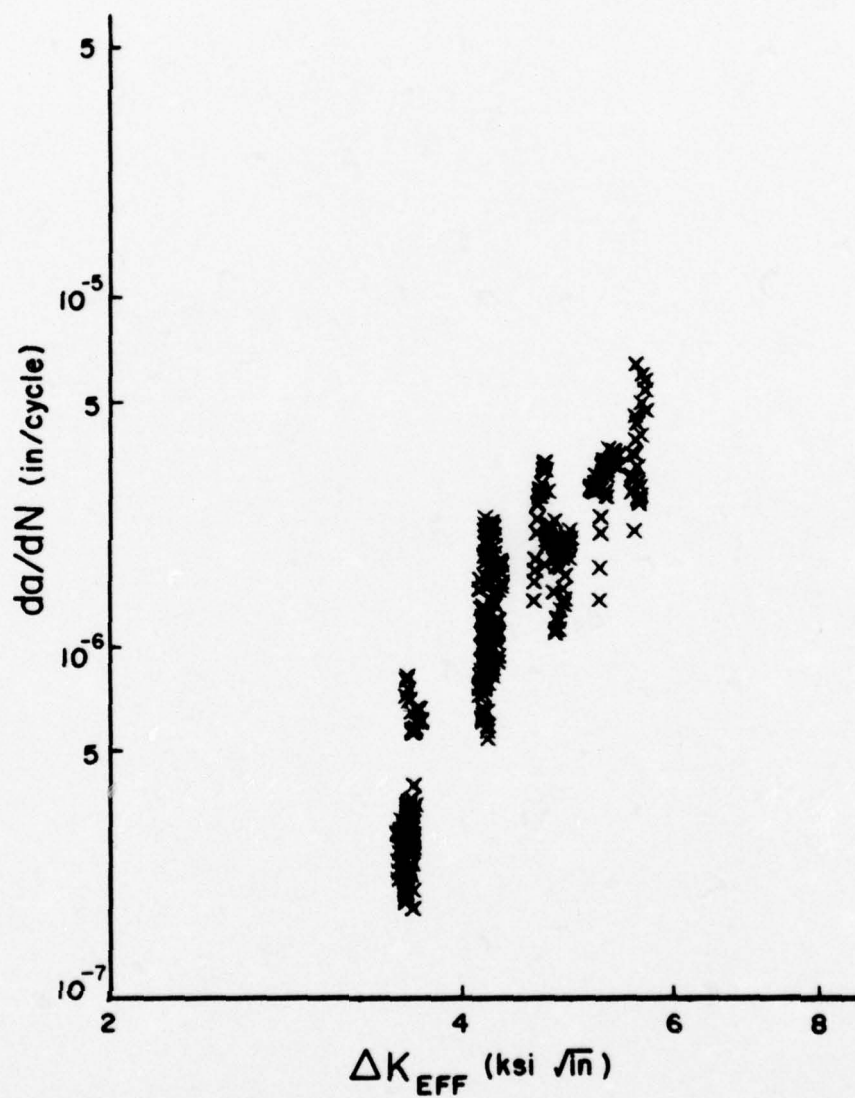
Figure 23   da/dN vs. ΔK_{EFF} for All Constant Amplitude Tests

A comparison of K_{OP} values obtained from Elber gage and inter-ferometry data is presented in Figure 24, where U versus R_F was plotted. The amount of scatter seems to be independent of the technique used to obtain K_{OP}. This suggests that conditions common to each test, conditions such as changes in the atmospheric conditions [27] or the definition of K_{OP} were responsible for much of the scatter. The effects of rigid body motions were observed in the reduction of the interferometry data. In these cases best fit curves were drawn graphically through the data points. Scatter was inherent in the interferometry data with rigid body motion present due to the sensi-tivity of the K_{OP} definition to the curvature of this best fit line.

Crack closure was measured by each technique for each R_F level investigated. Shih and Wei [10] observed no crack closure for R_F greater than 0.30. For these results at $R_F = 0.33$, K_{OP} was still 30 to 40 percent of the applied ΔK.

The trend was for K_{OP} to increase with ΔK as well as K_{MAX}. Some of the scatter which occurs with crack closure measurements can be attributed to differences in the fracture surfaces. Bachman and Munz [15] indicate that the straightness of the crack front has a major effect on K_{OP}. Ho et al. [13] suggest that the amount of closure increases with crack length. Irving et al. [12] observed the amount of closure was dependent on ΔK as well as crack length.

A second series of constant amplitude tests were performed at $R_F = 0.33$ with the same four ΔK as starting points. During these tests Elber gage measurements of P_{OP} were also taken at various gage locations relative to the crack tip. P_{OP} as a percent of the total
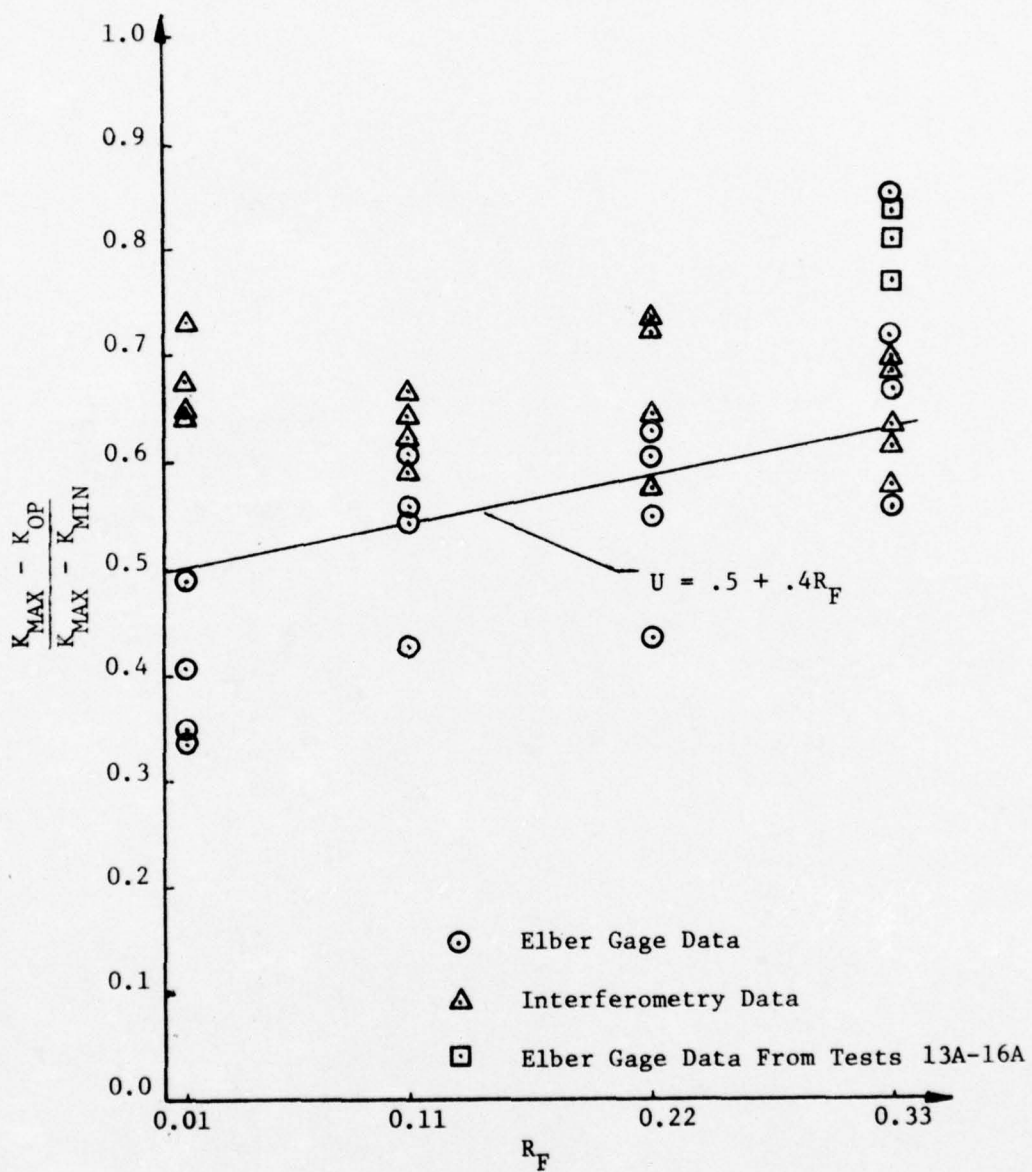
Figure 24 U vs. R_F Showing Interferometry and Elber Gage Data

load cycle was found to increase as the measurements were taken further behind the crack tip. P_{OP} values dropped off in a more abrupt fashion as the measurements were taken further ahead of the crack front. While gage location relative to the crack tip was not accurately measured this type of variation could easily account for discrepancies of $\pm$ 10 percent when compared to the value obtained at the tip. A summary of this limited investigation appears in Table 2, and is illustrated in Figure 25. It is also suspected that P_{OP} is dependent on overall crack length, however this investigation has not yielded sufficient data to confirm this effect.

The interferometry data exhibits slightly less scatter at each R level than the Elber gage data. This may be seen in Figure 24. The interferometry technique displayed great sensitivity to rigid body motions. The problem was most severe at low R levels. The value of K_{OP} obtained with the interferometry based method was consistently higher than the value obtained from Elber gage data.

It would have been desirable to digitize the load plus Elber gage and interferometry data for computer plotting of the load versus displacement curves. However for the limited amount of data collected in this investigation it would have only added complexity to the study.

The interferometry based technique permitting dynamic crack edge displacement measurements has been demonstrated to be a viable technique. It does however appear to be very sensitive to rigid body motions. It offers tremendous sensitivity especially when used near the crack tip. In the case of a linear trace (less than one complete cycle) the system was able to resolve displacements on the order of

Table 2

The Effect of Measurement Position on the Value of Crack Opening Load

ΔK (Ksi √in) Test Starting Level	P_{OP-5} % of Load Cycle	P_{OP-25} % of Load Cycle	K_{OP-5} (Ksi √in)	K_{OP-25} (Ksi √in)	Proximity to Crack Tip
5.5	43.04	22.78	5.27	4.11	Near
5.5	49.37	25.32	5.63	4.26	Behind
5.5	53.16	32.91	5.85	4.69	Far Behind
6.5	33.14	9.47	5.70	4.06	Ahead
6.5	34.32	23.08	5.78	5.01	Near
6.5	42.60	26.63	6.36	5.25	Behind
7.5	44.44	13.33	7.22	4.82	Ahead
7.5	48.89	18.89	7.57	5.25	Behind
8.5	40.43	12.77	7.98	5.52	Ahead
8.5	42.55	14.89	8.17	5.71	Near
8.5	44.68	17.02	8.36	5.90	Behind

NOTE: All tests are constant amplitude with $R_F = 0.33$. From the test starting level of ΔK cracks were grown approximately 0.500 mm prior to P_{OP} data being taken with the Elber gage.
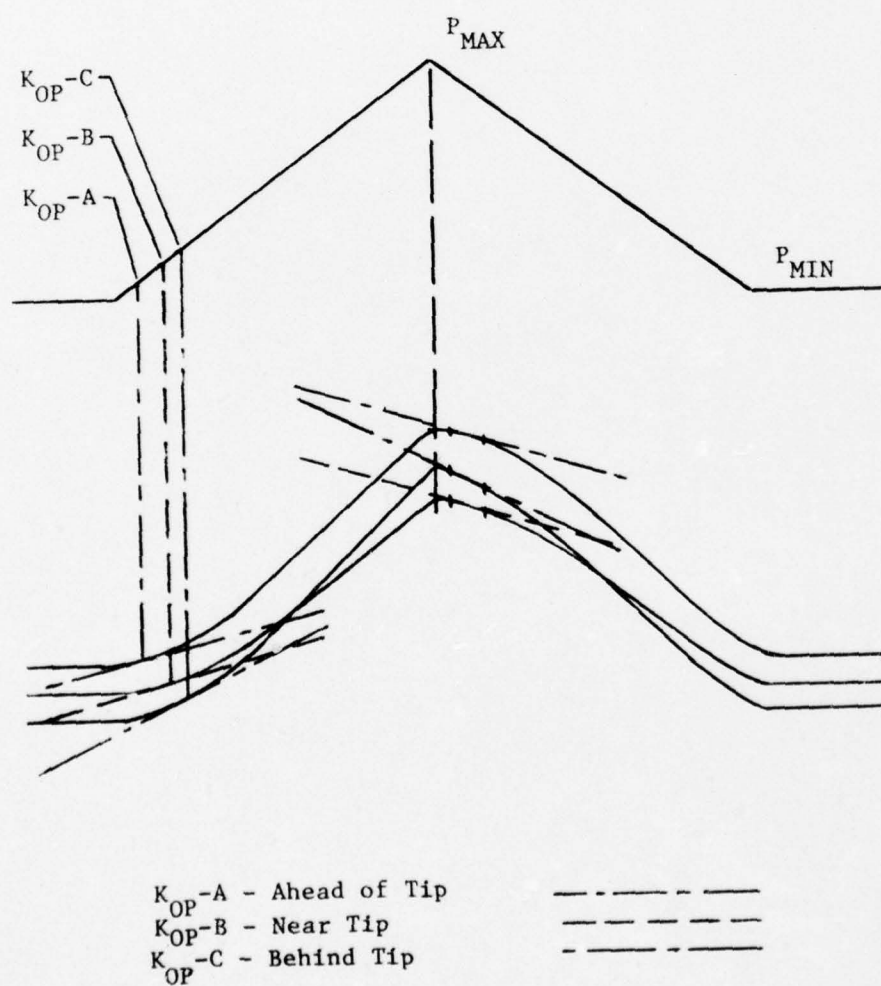
Figure 25 Effect of Proximity to Crack Tip on Measurement of K_{OP}.

0.01 microns. The Elber gage yielded good results with considerably less effort as a result it was used exclusively in the overload/ underload investigation.

Overload/Underload Test Results

It was the goal of this test program to measure K_{OP} after the application of an overload/underload sequence at a number of discrete points in the overload affected zone and compare this with K_{OP} determined using the inverse method. The results of this program are presented in Figures 26, 27, and 28. Alzos' original a versus N data is plotted in Figure B-1 in Appendix B. The 15 point strip technique of differentiation was used on this data to generate plots of da/dN versus a and K_{OP} versus a which appear as Figures B-1 and B-3 in Appendix B.

Arrest was defined as no crack growth for 10^6 cycles. Test 18 was expected to arrest and as a consequence it was planned to measure K_{OP} based on the number of cycles following the overload rather than on crack length. Delay behavior was anticipated in the remaining tests with K_{OP} measurements being planned based on crack length a. Crack length was observed to increase by varying amounts due to the application of the overload/underload sequences. After recording this value of a several Elber gage traces were recorded prior to performing the initial load shed. A minimum of one trace was necessary to adjust the strip chart recorder sensitivities. This is due to the inability of accurately and repeatably positioning the gage within a fixed distance of the crack tip. With an unassisted eye and the
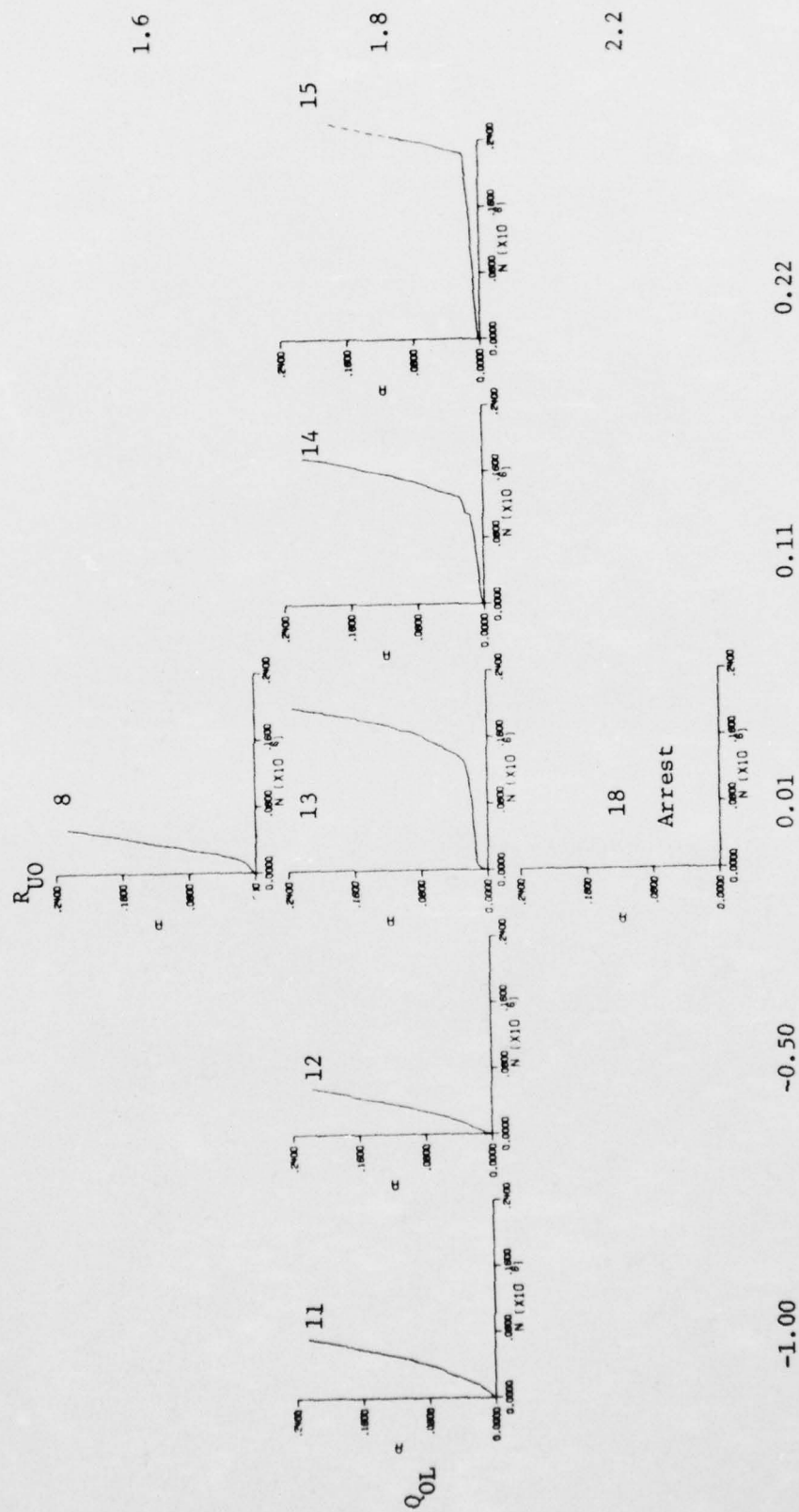
Figure 26 α vs. N for OL/UL Tests
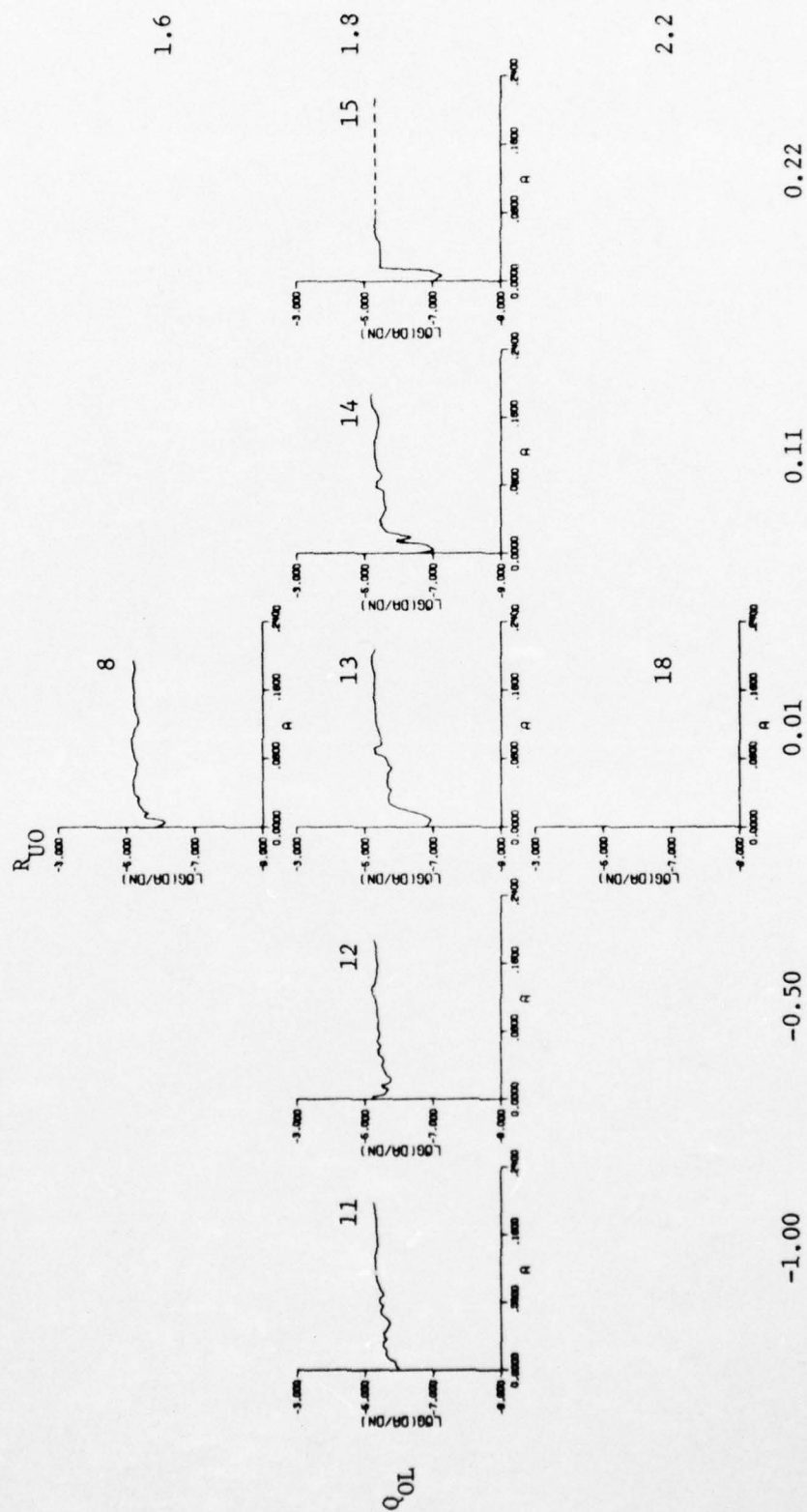
Figure 27 da/dN vs. a for OL/UL Tests Using 15 Point Moveable Strip Technique
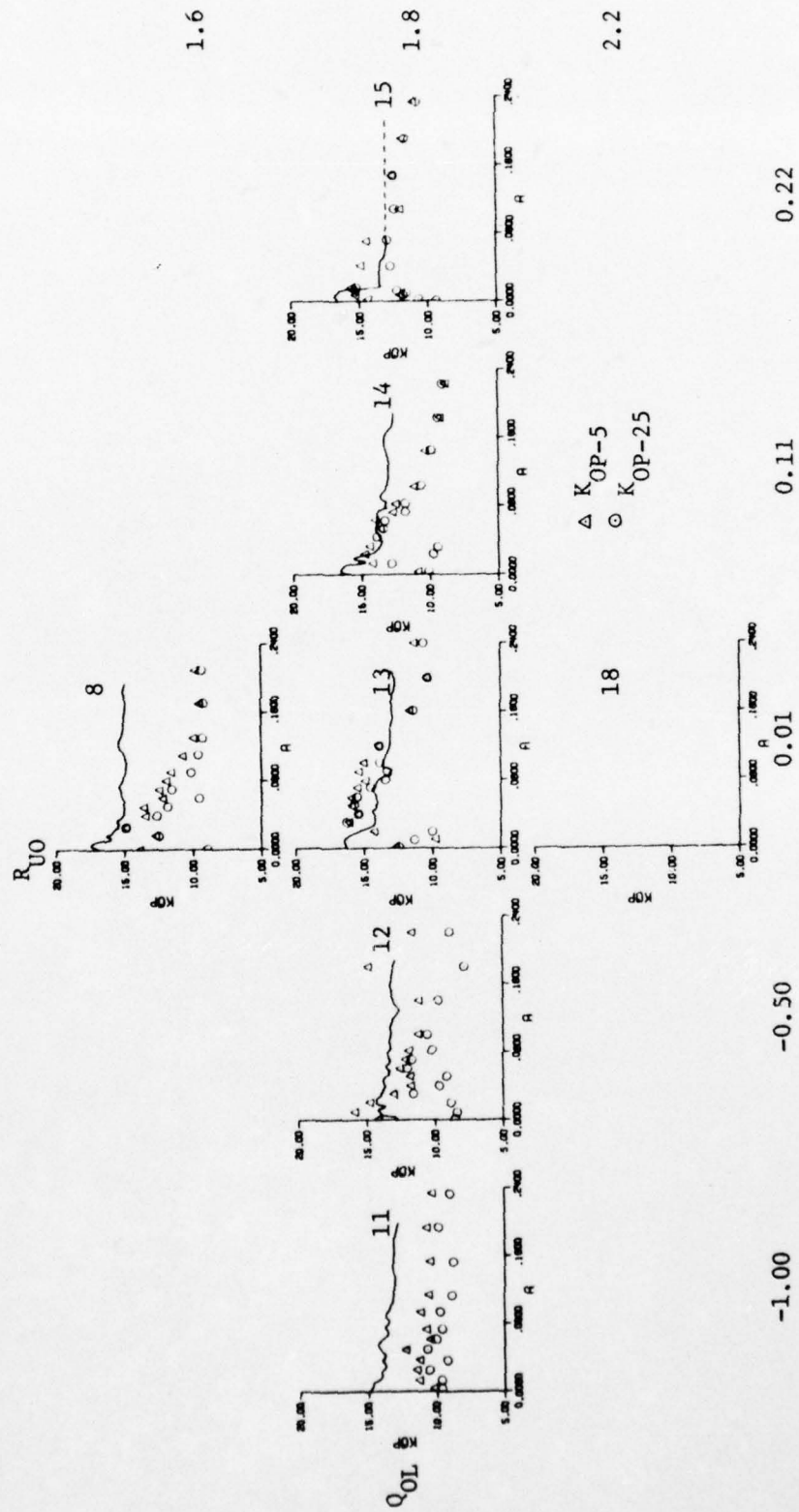
Figure 28 K_{OP} vs. a for OL/UL Tests

specimen at minimum load the crack tip is not always well defined or easily detected. With sensitivities adjusted two traces were taken at different chart paper speeds, the slower of these being better for qualitative shape comparisons and allowing determination of P_{OP-5}, with the faster chart speed being a better basis for data reduction allowing construction of a P vs. δ curve and determination of P_{OP-25}. Again measuring crack length after this series of single cycles generally revealed growth. This growth diminished as crack length increased in a given test, or as the crack grew out of the overload affected or plastic zone. Dynamic observation of crack length (machine cycling) gave a slightly different a value than would be observed staticly at minimum load. This could be caused by machine misalignment. Thus even the magnitude of this growth is subject to some uncertainty.

This growth could have its basis in one or more of the following: 1) Stopping the machine cycling drops the applied load in a nearly linear fashion from wherever the load is in the cycle. No suitable solution was found to eliminate this condition; 2) Rest times of several minutes at minimum load were required to change the function generator settings and position the Elber gage; 3) Changing the cyclic frequency by a factor of 1000 (20 Hz to 0.02 Hz) while data was taken may influence crack propagation behavior, especially in the overload affected zone near the point of the overload/underload application; 4) Changing the wave form from sinusoidal to triangular results in higher specimen accelerations at the troughs and peak of each cycle. This could influence subsequent growth behavior; and

5) Resumption of normal cycling probably does not result immediately in steady state growth behavior.

Test 18 was expected to arrest, however with each Elber gage trace taken crack growth was observed. This was probably attributable to some of the factors listed above. Subtracting this single cycle growth from the total indicated that the test could be classified as having arrested. Thus test 18 was terminated at approximately 700,000 cycles. The remaining tests exhibited the same qualitative behavior that Alzos observed but the number of cycles required for growth through the overload affected zone were from 2.1 to 4.3 times greater. The qualitative behavior based on a displayed good agreement. In the case of positive R_{UO} correlation based on the number of cycles is somewhat better. Based on three tests it is not possible to make any observations on the effect of Q_{OL}. Elber gage data was taken based on crack length in tests 8, 11, 12, 13, 14, and 15. The values of K_{OP} obtained from P_{OP-5} and P_{OP-25} displayed better agreement as steady state growth was approached near the end of the overload affected zone. Experimental K_{OP} results of tests 8, 11, 12, 13, 14, and 15 may be found in Tables B-2 through B-7 in Appendix B.

Crack growth observed after single cycling generally disappeared before the crack grew 1.5 mm past the overload crack length. In the region where single cycle growth was observed the Elber gage displayed hysteresis, i.e., would not return to zero.

Scatter in the data again may be a result of running in a non-controlled environment. Another source of scatter was the inability to take data repeatedly at the same distance from the crack tip.

Despite these problems the trends exhibited by the experimental K_{OP} values agree reasonably well with the inverse technique with K_{OP} giving slightly better agreement.

The a versus N data plotted in Figure 26 displays more abrupt transitions from delay to steady state behavior than Alzos's shown in Figure B-1. Growth rate, da/dN, versus a as well as K_{OP} versus a, shown in Figures 27 and 28, displays noticeably more variation than the corresponding plots in Figures B-2 and B-3. This was attributed to the repeated stopping, single cycling and starting necessary to collect K_{OP} data.

CONCLUSIONS

The most significant conclusions of this study are summarized
as follows:

1) Measurement of crack opening, K_{OP}, is a difficult experi-
   mental procedure at best. The method of data reduction,
   which depends on nonlinearities in the load displacement
   relationship, tends to introduce scatter because K_{OP} is not
   identified as a discrete point.

2) The laser interferometry system provides an accurate, convenient
   method for measuring crack opening displacements from which
   crack closure can be determined, however the data reduction
   with the system used in this investigation is time consuming.

3) The laser interferometry technique requires good specimen
   alignment and rigid fixturing to keep out of plane, rigid
   body motions to a minimum. This may have accounted for some
   of the scatter in the results of this study.

4) It has been shown, using the Elber gage, that crack opening
   load is dependent on the proximity of the measurement relative
   to the crack tip.

5) The measured values of K_{OP} following overload/underload sequences
   increased to a maximum then decreased to a steady state value.
   This compares favorably with the results obtained using the
   inverse technique and verifies previous qualitative explanations
   of load interaction effects.

RECOMMENDATIONS FOR FURTHER WORK

The concept of crack closure as investigated in this study has great potential for explaining fatigue crack propagation. Key to this understanding is the accurate measurement of K_{OP} and further investigation into its dependence on other test parameters. Based on observations made in connection with this investigation the following recommendations are made:

1) Research should be initiated to develop a measurement method or a definition of crack opening which identifies the magnitude of K_{OP} as a discrete quantity, as compared to the present definition of a tangency point on a curve.

2) On line, computer techniques for reducing the data should be developed for the laser interferometric system.

3) With crack opening displacement type measurements, the dependence of K_{OP} on the location of the measurement relative to the crack tip should be thoroughly investigated.

BIBLIOGRAPHY

BIBLIOGRAPHY

1. Willenborg, J., Engle, R.M., and Wood, H.A., "A Crack Growth Retardation Model Using an Effective Stress Concept," AFFDL-TM 71-1-FBR, 1971.

2. Wheeler, O.E., "Spectrum Loading and Crack Growth," Transactions of the ASME, Journal of Basic Engineering, 94 (March 1972), 181-186.

3. Elber, W., "Fatigue Crack Closure Under Cyclic Tension," Engineering Fracture Mechanics, 1970, Volume 2, pp. 37-45.

4. Elber, W., "The Significance of Fatigue Crack Closure," Damage Tolerance in Aircraft Structures, ASTM STP 486, American Society for Testing and Materials, 1971, pp. 230-242.

5. Alzos, W.X., "The Effects of Single Overload/Underload Cycles on Fatigue Crack Propagation," M.S. Thesis, Purdue University, May 1975.

6. Skat, A.C., Jr., "Evaluation of Extended Crack Closure in Fatigue Crack Delay Prediction for Single Overload/Underload Sequences," M.S. Thesis, Purdue University, May 1975.

7. Alzos, W.X., Skat, A.C., Jr., and Hillberry B.M., "Effect of Single Overload/Underload Cycles on Fatigue Crack Propagation," Fatigue Crack Growth Under Spectrum Loads, ASTM STP 595, American Society for Testing and Materials, 1976, pp. 41-60.

8. Paris, P.C. and Erdogan, F., "A Critical Analysis of Crack Propagation Laws," Transactions of the ASME, Journal of Basic Engineering, 85 (December 1963), 528-534.

9. Wei, R.P., Shih, T.T., and Fitzgerald, J.H., "Load Interaction Effects on Fatigue Crack Growth in Ti-6AL-4V Titanium Alloy," NASA CR-2239, 1973.

10. Wei, R.P. and Shih, T.T., "A Study of Crack Closure in Fatigue," NASA CR-2319, October 1973.

11. Crandall, G.M., "Residual Stress Intensity Parameters for Prediction of Delay in Fatigue Crack Propagation," M.S. Thesis, Purdue University, December 1975.

12. Irving, E., Robinson, J.L. and Beevers, C.J., "Fatigue Crack Closure in Titanium and Titanium Alloys," International Journal of Fracture, Volume 9, 1973, pp. 105-108.

13. Ho, C.L., Buck, O., and Marcus, H.L., "Application of Strip Model to Crack Tip Resistance and Crack Closure Phenomena," Progress in Flaw Growth and Fracture Toughness Testing, ASTM STP 536, American Society for Testing and Materials, 1973, pp. 5-21.

14. Roberts, R. and Schmidt, "Observations of Crack Closure," International Journal of Fracture Mechanics, Volume 8, 1972, pp. 469-471.

15. Bachman, V. and Munz, D., "Crack Closure in Fatigue of a Titanium Alloy," International Journal of Fracture, Volume 11, 1975, pp. 713-716.

16. Katcher, M. and Kaplan, M., "Effects of R-Factor and Crack Closure on Fatigue Crack Growth for Aluminum and Titanium Alloys," Fracture Toughness and Slow-Stable Cracking, ASTM STP 599, American Society for Testing and Materials, 1974, pp. 264-282.

17. Adams, N.J., Fatigue Crack Closure at Positive Stresses", Engineering Fracture Mechanics, 5, Volume 1, 1973, pp. 543-554.

18. Pitoniak, F. J., Grandt, A. F. Jr., Montulli, L. T., and Packman, P. F., "Fatigue Crack Retardation and Closure in Polymethylmethacrylate," Engineering Fracture Mechanics, 1974, Volume 6, pp. 663-670.

19. Sharpe, W.N., Jr. and Grandt, A.F., Jr., "A Laser Interferometric Technique for Crack Surface Displacement Measurement," AFML-TR-74-75, Air Force Materials Laboratory, Wright-Patterson Air Force Base, Ohio, July 1974.

20. Sharpe, W.N., Jr., and Grandt, A.F., Jr., "A Preliminary Study of Fatigue Crack Retardation Using Laser Interferometry to Measure Crack Surface Displacements," Mechanics of Crack Growth, ASTM STP 590, American Society for Testing and Materials, 1976, pp. 302-320.

21. Macha, D.E., Sharpe, W.N., Jr. and Grandt, A.F., Jr., "A Laser Interferometry Method for Experimental Stress Intensity Factor Calibration," Ninth National Symposium on Fracture Mechanics, University of Pittsburgh, Pittsburgh, PA, August 25-27, 1975.

22. Sharpe, W.N., Jr., Corbly, D.M. and Grandt, A.F., Jr., "The Effects of Rest-Time on Fatigue Crack Retardation and Observations of Crack Closure," AFML-TR-75-57, Air Force Materials Laboratory, Wright-Patterson Air Force Base, Ohio, August 1975.

23. Probst, E.P. and Hillberry, B.M., "Fatigue Crack Delay and Arrest Due to Single Peak Tensile Overloads," AIAA Journal, Volume 12, No. 3, 1974, pp. 330-335.

24. Himmelein, M.K., "The Effect of Stress Ratio and Overload Ratio on Fatigue Crack Delay and Arrest Behavior Due to Single Peak Overloads," M.S. Thesis, Purdue University, 1974.

25. Tada, H., Paris, P., and Irwin, G., The Stress Analysis of Cracks Handbook, Del Research Corporation, Hellertown, Pennsylvania, 1973.

26. Fowles, G.R., Introduction to Modern Optics, Holt Rinehart and Winston Inc., 1968, pp. 63-67.

27. Hsu, T.M. and Lassiter, L.W., "Effects of Compressive Overloads on Fatigue Crack Growth," AIAA Paper No. 74-365, April 1974.

APPENDIX A

MICROCOPY RESOLUTION TEST CHART

NATIONAL BUREAU OF STANDARDS 1963
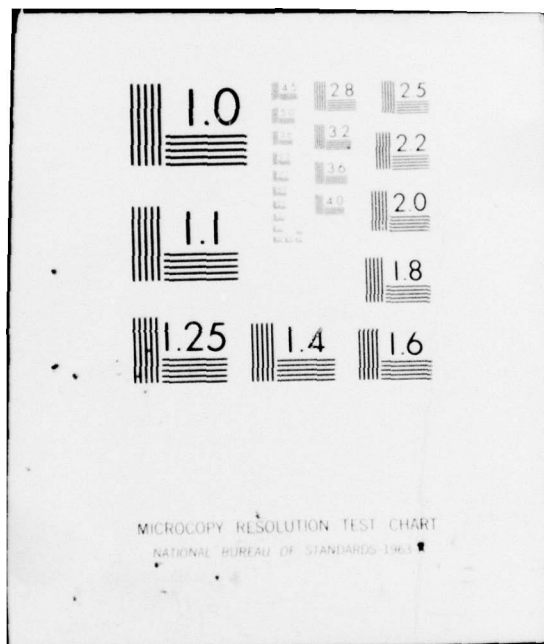
Table A-1

Constant Amplitude Test Results

Test Number	R_F	$a_{K_{OP}}$ (mm)	K_{MAX} (Ksi √in)	P_{OP} as a percent of $P_{MAX}-P_{MIN}$		K_{OP} (Ksi √in)		$U = \dfrac{K_{MAX}-K_{OP}}{\Delta K}$	
				E.G.	I.D.M.	E.G.	I.D.M.	E.G.	I.D.M.
1	0.01	6.615	7.34	32.32	58.99	2.42	4.36	0.68	0.41
2		7.940	8.61	35.58	64.90	3.12	5.62	0.64	0.35
3		9.600	9.51	26.59	66.00	2.60	6.31	0.73	0.34
4		12.084	10.46	34.95	50.98	3.73	5.39	0.65	0.49
5	0.11	14.330	7.46	33.33	57.17	3.03	4.62	0.67	0.43
6		15.000	8.57	35.29	45.28	3.63	4.40	0.65	0.55
7		16.350	10.02	40.69	39.19	4.73	4.60	0.59	0.61
8		17.300	10.94	37.50	44.05	4.85	5.49	0.63	0.56
9	0.22	18.940	7.81	42.11	45.05	4.28	4.46	0.58	0.55
10		19.506	9.11	35.19	56.30	4.50	6.00	0.65	0.44
11		21.220	10.43	27.36	39.29	4.52	5.49	0.73	0.61
12		22.000	11.74	26.23	36.88	4.99	5.96	0.74	0.63
13	0.33	21.550*	8.29	36.36	14.40	4.75	3.53	0.64	0.86
14		9.300	10.55	33.86	45.00	5.46	6.66	0.72	0.68
15		20.150*	11.31	41.87	32.98	6.91	6.23	0.58	0.67
16		21.030*	12.72	30.01	44.07	6.76	7.95	0.70	0.56
13A	0.33	6.520	8.52	22.78	–	4.11	–	0.77	–
14A		7.750	10.33	23.08	–	5.01	–	0.77	–
15A		8.900	11.51	18.89	–	5.25	–	0.81	–
16A		10.600	13.28	14.89	–	5.71	–	0.85	–

* Denotes an eccentric crack and a lower than expected growth rate.

No interferometry data was taken for test 13A, 14A, 15A and 16A.

NOTE: E.G. = Elber Gage, I.D.M. = Interferometry Displacement Measurement

Figure A-1 Constant stress amplitude data (showing alternate

points only) and least square fit line for

Equation 4   where $\Delta K_{EFF} = 0.5 + 0.4R_F$

APPENDIX B

Table B-1

Alzos' Overload/Underload Tests and Results

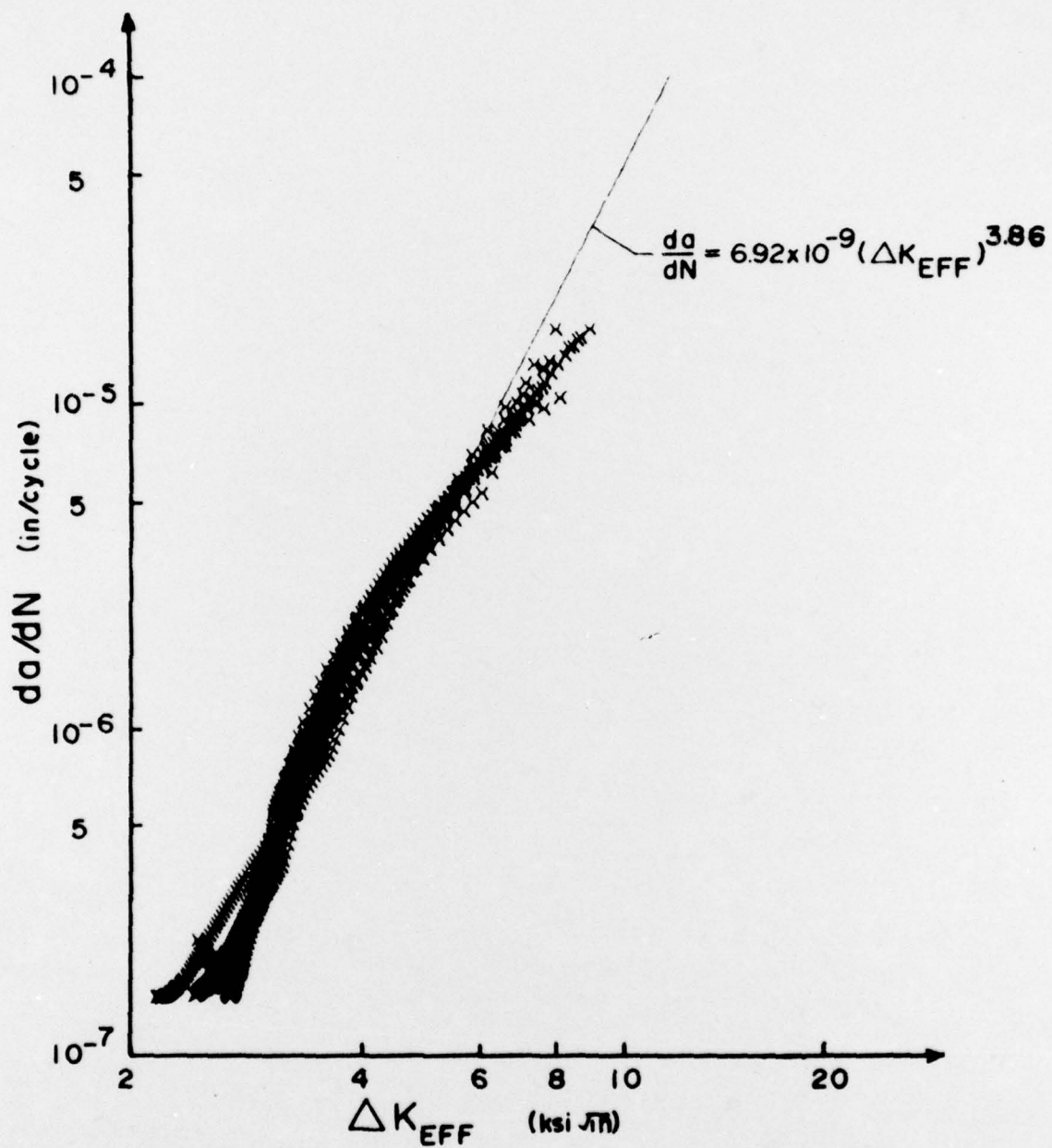| Test No.	K_{MAX} (ksi√in)	ΔK (ksi√in)	R_F	Q_{OL}	R_{UO}	R_M	$\frac{da}{dN}\bigg\vert_{SS}$ PRE. O.L. (in/cycle)	$\frac{da}{dN}\bigg\vert_{SS}$ POST O.L. (in/cycle)	$\frac{da}{dN}\bigg\vert_{MIN}$ (in/cycle)	N_D (cycles)	Δa^* (in)	a_{OL} (in)	Spec.
1	33.33	11.67	0.65	1.00	0.11	0.65	2.58×10^{-5}	2.60×10^{-5}	2.60×10^{-5}	0	0	0.67	A-1
2	25.64	11.50	0.55	1.30	0.11	0.42	2.04×10^{-5}	2.12×10^{-5}	3.65×10^{-6}	6,800	0.061	0.94	A-1
3	20.83	11.50	0.45	1.60	0.11	0.28	1.39×10^{-5}	1.41×10^{-5}	7.76×10^{-7}	22,000	0.079	1.23	A-1
4	17.54	11.50	0.34	1.90	0.11	0.18	1.19×10^{-5}	1.00×10^{-5}	1.86×10^{-7}	121,000	0.138	0.81	A-2
5	15.15	11.50	0.24	2.20	0.11	0.11	6.53×10^{-6}	-	-	-	-	?.23	A-2
6	20.83	13.50	0.35	1.60	-1.00	0.22	4.04×10^{-5}	3.55×10^{-5}	9.65×10^{-6}	5,850	0.080	1.57	A-5
7	20.83	13.50	0.35	1.60	-0.50	0.22	2.48×10^{-5}	2.66×10^{-5}	5.02×10^{-6}	10,600	0.103	1.46	A-3
8	20.83	13.50	0.35	1.60	0.01	0.22	2.29×10^{-5}	1.78×10^{-5}	2.93×10^{-6}	11,400	0.074	0.84	A-3
9	20.83	13.50	0.35	1.60	0.11	0.22	1.79×10^{-5}	2.00×10^{-5}	2.12×10^{-6}	18,400	0.093	0.49	A-3
10	20.83	13.50	0.35	1.60	0.22	0.22	1.88×10^{-5}	1.78×10^{-5}	5.29×10^{-7}	44,000	0.093	0.52	A-10
11	18.52	11.19	0.40	1.80	-1.00	0.22	1.39×10^{-5}	1.58×10^{-5}	4.31×10^{-6}	11,800	0.074	1.07	A-5
12	18.52	11.19	0.40	1.80	-0.50	0.22	1.94×10^{-5}	1.41×10^{-5}	4.01×10^{-6}	14,400	0.093	0.70	A-5
13	18.52	11.19	0.40	1.80	0.01	0.22	1.24×10^{-5}	1.00×10^{-5}	9.34×10^{-7}	42,600	0.127	0.43	A-6
14	18.52	11.19	0.40	1.80	0.11	0.22	1.16×10^{-5}	1.00×10^{-5}	2.55×10^{-7}	53,000	0.102	1.17	A-4
15	18.52	11.19	0.40	1.80	0.22	0.22	1.12×10^{-5}	1.20×10^{-5}	1.07×10^{-7}	142,000	0.120	0.81	A-6
16	15.15	7.82	0.48	2.20	-1.00	0.22	4.76×10^{-6}	5.01×10^{-6}	1.05×10^{-6}	52,000	0.110	1.27	A-6
17	15.15	7.82	0.48	2.20	-0.50	0.22	6.55×10^{-6}	7.94×10^{-6}	1.92×10^{-7}	127,000	0.170	1.40	A-10
18+	15.15	7.82	0.48	2.20	0.01	0.22	4.88×10^{-6}	-	-	-	-	1.45	A-8
19+	15.15	7.82	0.48	2.20	0.11	0.22	5.93×10^{-6}	-	-	-	-	0.67	A-13
20+	15.15	7.82	0.48	2.20	0.22	0.22	4.81×10^{-6}	-	-	-	-	1.64	A-6
21	18.52	14.85	0.20	1.80	-1.00	0.11	2.18×10^{-5}	1.78×10^{-5}	5.36×10^{-6}	10,300	0.078	1.11	A-13
22	18.52	14.85	0.20	1.80	-0.05	0.11	3.10×10^{-5}	1.41×10^{-5}	4.41×10^{-6}	17,600	0.125	0.41	A-9
23	18.52	14.85	0.20	1.80	0.01	0.11	2.32×10^{-5}	1.78×10^{-5}	3.29×10^{-7}	44,500	0.068	1.70	A-8
24	18.52	14.85	0.20	1.80	0.11	0.11	2.02×10^{-5}	2.00×10^{-5}	3.54×10^{-7}	63,700	0.137	0.43	A-7
30	18.52	8.52	0.54	1.80	-1.00	0.30	7.59×10^{-6}	7.24×10^{-6}	1.06×10^{-6}	25,000	0.093	2.03	A-6
31	18.52	8.52	0.54	1.80	-0.50	0.30	9.61×10^{-6}	7.94×10^{-6}	2.39×10^{-6}	17,600	0.065	0.97	A-10
32	18.52	8.52	0.54	1.80	0.01	0.30	6.67×10^{-6}	6.31×10^{-6}	5.90×10^{-7}	52,800	0.059	0.47	A-8
33	18.52	8.52	0.54	1.80	0.11	0.30	6.31×10^{-6}	6.33×10^{-6}	2.81×10^{-7}	83,200	0.118	0.74	A-8
34	18.52	8.52	0.54	1.80	0.22	0.30	6.33×10^{-6}	7.08×10^{-6}	1.03×10^{-7}	197,000	0.123	0.98	A-8
35	18.52	8.52	0.54	1.80	0.30	0.30	7.08×10^{-6}	-	-	-	-	1.21	A-8
16-2.4+	13.89	6.56	0.53	2.40	-1.00	0.22	3.88×10^{-6}	2.82×10^{-6}	3.14×10^{-7}	124,000	0.113	1.64	A-13
16-2.6	12.82	5.49	0.57	2.60	-1.00	0.22	1.52×10^{-6}	2.63×10^{-6}	1.27×10^{-7}	260,000	0.115	1.09	A-14
17-2.4	13.89	6.56	0.53	2.40	-0.50	0.22	3.57×10^{-6}	2.14×10^{-6}	5.55×10^{-7}	126,000	0.137	0.45	A-14
3A/D-.4a+	11.11	7.78	0.30	3.00	-0.40	0.10	5.15×10^{-6}	-	-	-	-	1.56	A-14
3A/D-.4b+	11.11	7.78	0.30	3.00	-0.40	0.10	4.00×10^{-6}	-	-	-	-	0.72	A-15
3A/D-.5	11.11	7.78	0.30	3.00	-0.50	0.10	4.93×10^{-6}	2.82×10^{-6}	1.05×10^{-7}	593,000	0.150	0.48	A-15
R-12	18.52	11.19	0.40	1.80	-0.50	0.22	4.02×10^{-5}	1.00×10^{-5}	7.72×10^{-8}	160,550	0.089	0.52	A-12
R-13	18.52	11.19	0.40	1.80	0.01	0.22	1.05×10^{-5}	9.33×10^{-6}	1.52×10^{-7}	169,000	0.100	0.48	A-11

* Tests 25-29 are the same as Tests 11-15

+ Tests arrested - $N_D > 10^6$ cycles; $\frac{da}{dN}\big\vert_{MIN} < 4 \times 10^{-10}$ in/cycles

NOTE: $K_{OL} = 33.33$ ksi√in for all Tests.

   $2r_y = 0.109$ in for all Tests.

   Overload Preceeded Underload Except in Tests R-12, R-13.

Table B-2

Elber Gage Crack Opening Data For Overload/Underload Test 8
a_{OL} = 21.500 mm

Normalized Crack Length (mm)	P_{OP-25} (% $P_{MAX}-P_{MIN}$)	K_{OP-25} (Ksi $\sqrt{in}$)	P_{OP-5} (% $P_{MAX}-P_{MIN}$)	K_{OP-5} (Ksi $\sqrt{in}$)
0.00	12.50	9.02	48.96	13.94
0.40	38.54	12.53	39.58	12.67
0.65	56.25	14.92	56.25	14.92
1.00	39.58	12.67	45.83	13.52
1.25	34.04	11.93	46.81	13.65
1.50	17.02	9.63	36.17	12.21
1.75	31.91	11.64	38.30	12.50
2.00	23.40	10.49	34.04	11.93
2.25	21.28	10.20	31.91	11.64
2.75	17.02	9.63	25.53	10.78
3.25	15.22	9.38	17.39	9.68
4.25	14.35	9.27	15.91	9.48
5.25	15.12	9.37	18.60	9.84

Table B-3

Elber Gage Crack Opening Data For Overload/Underload Test 11
a_{OL} = 21.000 mm

Normalized Crack Length (mm)	P_{OP-25} (% $P_{MAX}-P_{MIN}$)	K_{OP-25} (Ksi $\sqrt{in}$)	P_{OP-5} (% $P_{MAX}-P_{MIN}$)	K_{OP-5} (Ksi $\sqrt{in}$)
0.06	19.36	9.50	24.19	10.04
0.30	19.51	9.51	34.15	11.15
0.60	28.05	10.47	35.37	11.29
0.90	16.05	9.13	33.33	11.06
1.20	29.11	10.59	42.18	12.05
1.50	22.78	9.88	26.68	10.32
1.80	18.99	9.46	29.11	10.59
2.30	20.78	9.66	33.77	11.04
2.80	12.99	8.78	27.69	10.43
3.80	12.16	8.69	27.03	10.35
4.80	22.22	9.82	29.17	10.59
5.80	14.29	8.93	25.71	10.21

Table B-4

Elber Gage Crack Opening Data For Overload/Underload Test 12
a_{OL} = 12.500 mm

Normalized Crack Length (mm)	P_{OP-25} (% $P_{MAX}-P_{MIN}$)	K_{OP-25} (Ksi $\sqrt{in}$)	P_{OP-5} (% $P_{MAX}-P_{MIN}$)	K_{OP-5} (Ksi $\sqrt{in}$)
0.02	9.62	8.41	59.62	14.00
0.25	8.65	8.30	75.47	15.78
0.50	12.26	8.71	65.38	14.65
0.75	37.50	11.53	50.00	12.93
1.00	20.19	9.59	38.46	11.63
1.25	15.38	9.05	38.46	11.63
1.50	40.78	11.89	44.66	12.33
1.75	37.86	11.57	41.40	11.96
2.04	25.32	10.16	40.00	11.81
2.50	28.00	10.46	34.00	11.13
3.50	20.83	9.66	33.33	11.06
4.50*	4.44	7.83	66.67	14.79
5.50	13.33	8.82	37.78	11.56

* Poor trace.

Table B-5

Elber Gage Crack Opening Data For Overload/Underload Test 13
a_{OL} = 8.000 mm

Normalized Crack Length (mm)	P_{OP-25} (% $P_{MAX}-P_{MIN}$)	K_{OP-25} (Ksi $\sqrt{in}$)	P_{OP-5} (% $P_{MAX}-P_{MIN}$)	K_{OP-5} (Ksi $\sqrt{in}$)
0.045	45.59	12.43	47.06	12.60
0.25	35.29	11.28	20.59	9.63
0.50	24.01	10.02	61.52	14.21
0.75	79.53	16.23	78.03	16.06
1.00	72.03	15.39	72.03	15.39
1.25	75.00	15.72	76.56	15.90
1.50	72.88	15.49	76.56	15.90
1.75	64.52	14.55	72.58	15.45
2.00	54.84	13.47	67.74	14.91
2.25	55.00	13.48	71.67	15.35
2.50	58.33	13.85	68.33	14.98
3.00	58.62	13.89	58.62	13.89
4.00	35.71	11.33	38.07	11.59
5.00	26.61	10.31	26.61	10.31
6.00	29.41	10.62	35.29	11.28

Table B-6

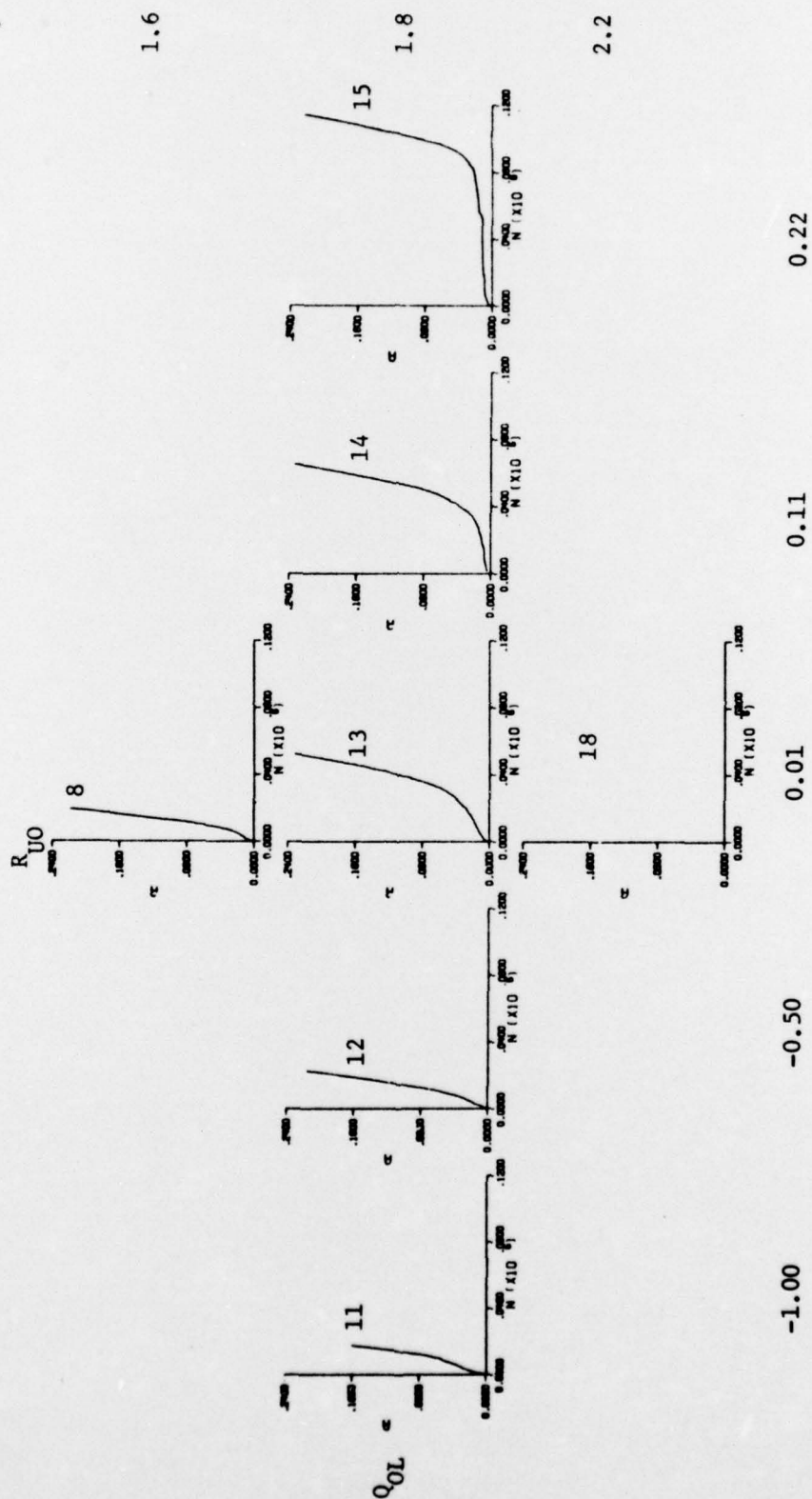Elber Gage Crack Opening Data For Overload/Underload Test 14
a_{OL} = 15.220 mm

Normalized Crack Length (mm)	P_{OP-25} (% P_{MAX}-P_{MIN})	K_{OP-25} (Ksi $\sqrt{in}$)	P_{OP-5} (% P_{MAX}-P_{MIN})	K_{OP-5} (Ksi $\sqrt{in}$)
0.08	25.00	10.13	31.25	10.83
0.33	48.96	12.81	61.46	14.21
0.58	21.88	9.78	65.63	14.67
0.83	18.75	9.43	62.50	14.32
1.08	58.95	13.93	58.95	13.93
1.33	54.74	13.46	55.54	13.54
1.58	53.26	13.29	59.39	13.98
1.83	40.22	11.83	47.83	12.68
2.08	40.22	11.83	45.65	12.44
2.58	29.83	10.67	33.59	11.09
3.58	22.73	9.87	27.27	10.38
4.58	18.60	9.41	17.44	9.28
5.58	15.48	9.06	14.29	8.93

Table B-7

Elber Gage Crack Opening Data For Overload/Underload Test 15
a_{OL} = 17.100 mm

Normalized Crack Length (mm)	P_{OP-25} (% P_{MAX}-P_{MIN})	K_{OP-25} (Ksi $\sqrt{in}$)	P_{OP-5} (% P_{MAX}-P_{MIN})	K_{OP-5} (Ksi $\sqrt{in}$)
0.00	19.15	9.47	31.91	10.90
0.08	29.60	10.64	62.22	14.29
0.18	39.72	11.77	70.61	15.23
0.22	37.51	11.53	41.92	12.02
0.32	44.13	12.27	71.71	15.35
0.42	70.61	15.23	72.82	15.48
1.05	48.54	12.76	67.30	14.86
1.76	50.00	12.93	63.64	14.45
2.70	46.17	12.50	41.55	11.98
3.68	46.51	12.53	46.51	12.53
4.75	38.75	11.67	40.00	11.81
5.83	31.04	10.80	33.63	11.09

Figure B-1 α vs. N For Alzos' Overload/Underload Tests
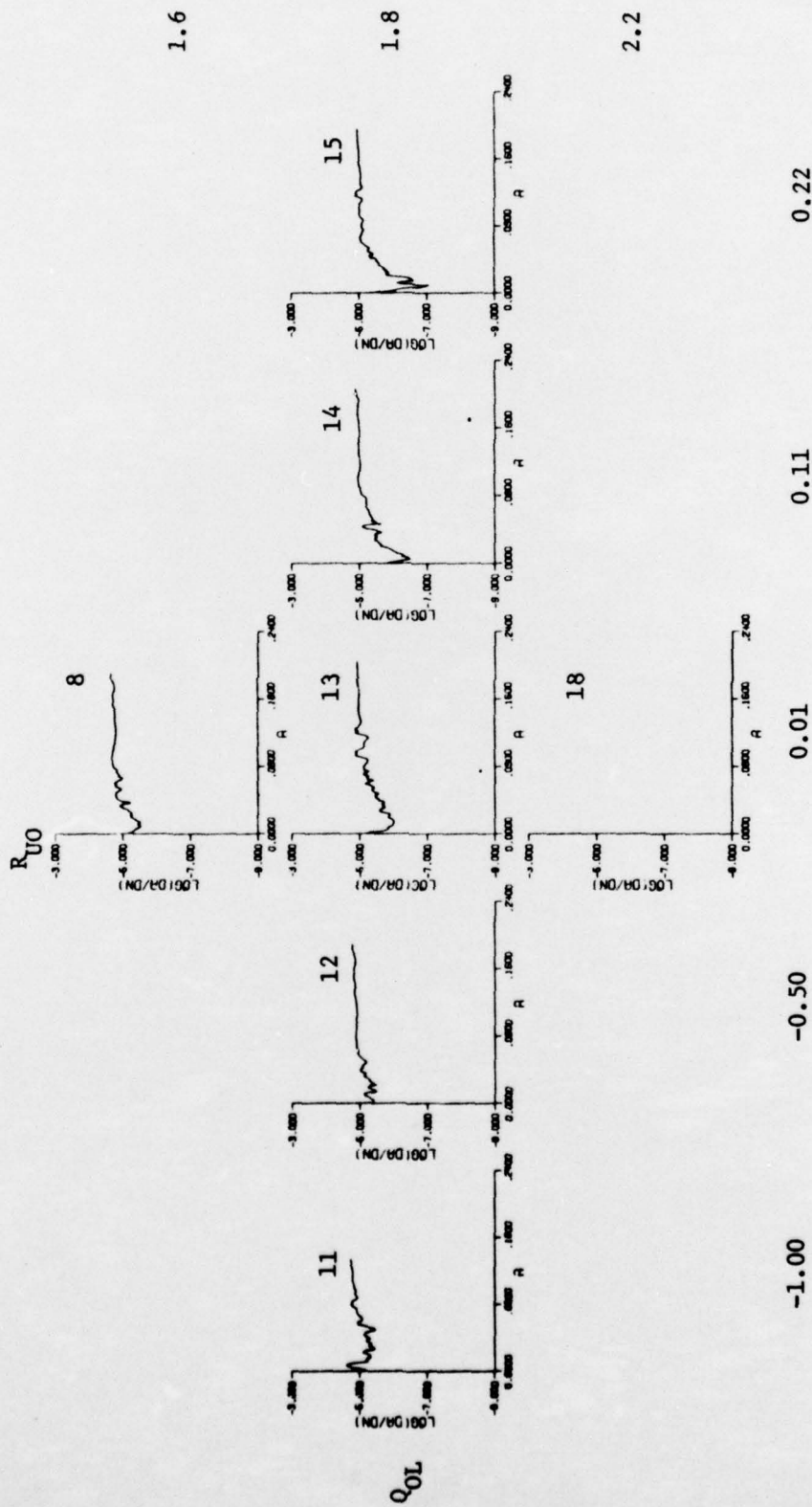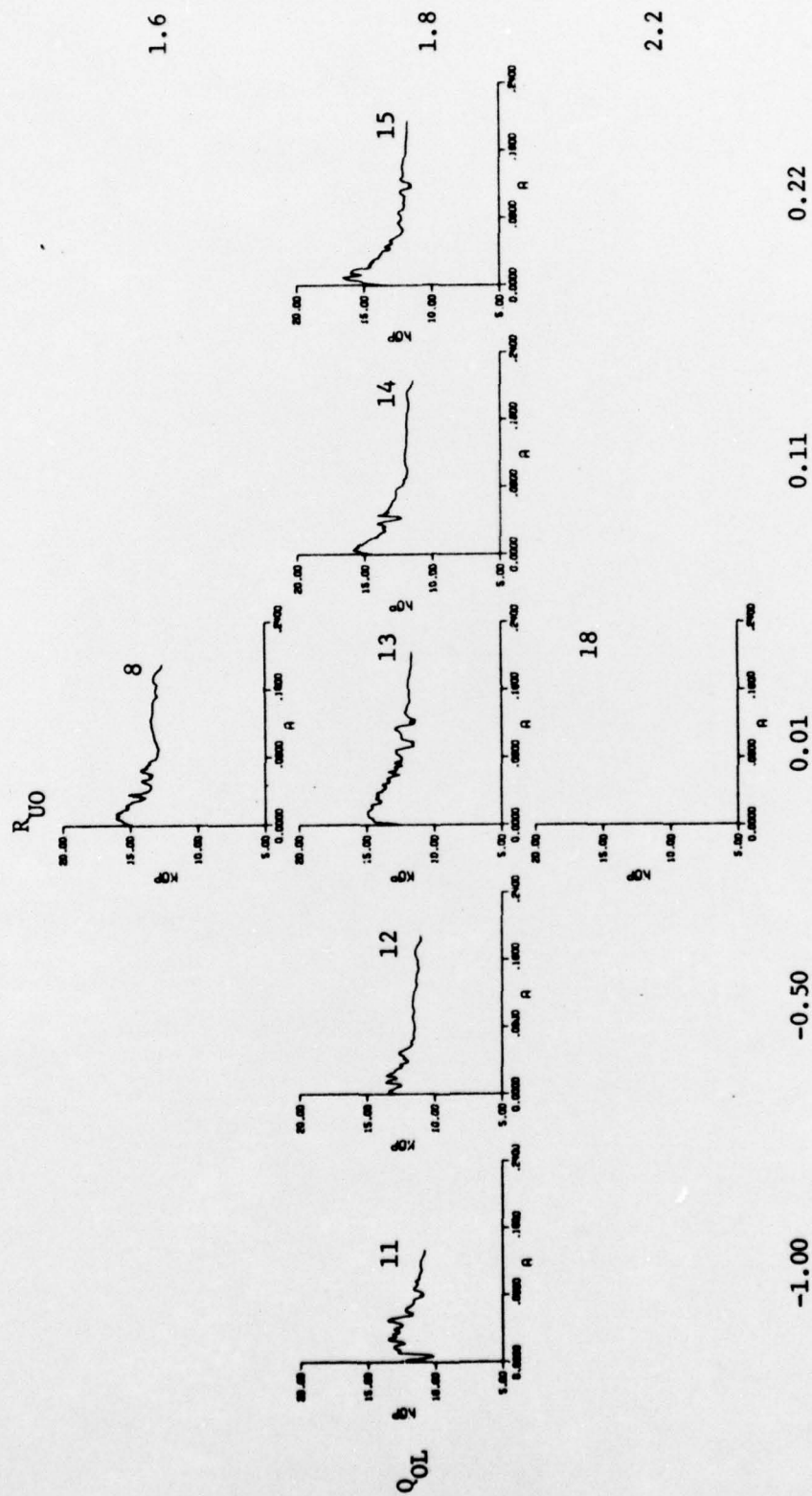
Figure B-2 Log dα/dN vs. α For Alzos' Overload/Underload Tests

Figure B-3 K_{OP} vs. a For Alzos' Overload Underload Tests